"In the 20th century, widespread electrification gave us power for our cities, factories, farms, and homes - and forever changed our lives. Thousands of engineers made it happen, with innovative work in fuel sources, power generating techniques, and transmission grids. From street lights to supercomputers, electric power makes our lives safer, healthier, and more convenient."

– The National Academy of Engineering, 2000

3. Introduction

3.1. Towards the Greenfield Approach

The National Academy of Engineering named the electric power grid the greatest engineering achievement of the 20th century [1]. However, as recent large-scale power grid failures illustrate, the (electro-mechanical) electric grid is being operated closer and closer to its limits. Specifically, the electric grid of the 20th century is aging and congested. Furthermore, it will not be able to meet future demands without operational changes and significant capital investments over the next decades [2]. Thus, the electric grid of the 21st century represents an open problem for the research community and industry. With the development of new technologies, such as, flexible AC transmission devices (FACTS), phasor measurement units (PMUs), renewable and distributed generation, flexible loads, and energy storage solutions, the tools are available to enable a paradigm shift for the electric grid.

To overcome the limitations of today's power grid, two main approaches are considered by engineers and scientists. The first approach investigates improvements to energy-delivery systems subject to boundary conditions given by today's grid structures. The second approach seeks to develop and design a new paradigm for optimal future energy delivery systems, which takes into account novel emerging technologies. By treating the second approach (i.e. the greenfield approach) as the forecasted optimal 'target' system, the first approach can be considered a coordinated effort to bridge today's aging and congested system with the optimal future target system, as Fig. 1 illustrates.

The design and development of the greenfield approach can be considered the long-term goal of power systems engineers and scientists, while the bridging approach can be considered a series of short-term projects. It is within this framework that the work is developed in this chapter. Namely, we build upon the ETH Zürich project *"Vision for Future Energy Networks,"* which
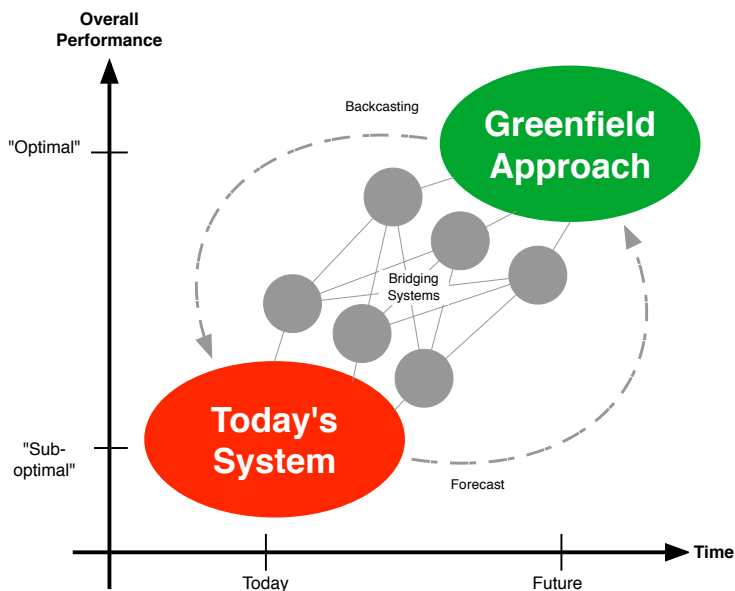
Figure 1: Designing a future greenfield approach allows us to move from today's aging and congested power system to the future optimal system. Figure is inspired from [3].

focused on a synergistic interconnected energy systems model as their greenfield approach. To accomplish the interconnection of energy systems, the ETH project developed modeling tools such as the 'energy hub' and multi-energy carriers and analyzed many scenarios under the new multi-energy context, see [3, 4, 5].

This chapter expands upon the ETH project by employing the 'energy hub' as a generic energy storage device to analyze the performance of energy delivery systems with energy storage in contingency scenarios (i.e. under unscheduled line outages). This is achieved by developing a novel model-predictive control (MPC) scheme that ensures efficient operation of energy systems and mitigates the effects of severe line-outage disturbances through feedback algorithms. Developed algorithms are illustrated through a comprehensive simulation study. The interdisciplinary research presented in this chapter lies at the intersection of power systems, optimization, and controls. Specifically, a model-predictive control-based cascade mitigation approach is analyzed herein. The approach is developed into a practical, yet rigorously justified, cascade mitigation scheme for the electric bulk power system.

3.2. Cascade-mitigation

Currently, abnormal conditions are handled either through protection operation or operator intervention, depending on the severity of the abnormality. In the latter case, where conditions do not immediately threaten the integrity of plant or loads, operators institute corrective procedures that may include altering generation schedules, adjusting transformer tap positions, and switching capacitors/reactors. For more extreme abnormalities, the protection associated with vulnerable components will operate to ensure they do not suffer damage. This myopic response may, however, weaken the network, exacerbating the conditions experienced by other components. They may subsequently trip, initiating an uncontrolled cascade of outages. This pattern was exhibited during the blackout of the U.S. and Canada in August 2003 [6].

As the amount, type and distribution of controllable resources increases, operators will find it ever more challenging to determine an appropriate response to unanticipated events. At a minimum, operators will require new tools to guide their decision-making. Given the increased complexity of response actions, a closed-loop feedback process will become indispensable. Furthermore, since power systems are suffused with constraints and limits on states and inputs, model predictive control (MPC) schemes can be particularly useful within the context of contingency management. For a general overview of MPC, see [7, 8, 9].

The first application of MPC to emergency control of power systems was [10], where voltage stability was achieved through optimal coordination of load shedding, capacitor switching, and tap-changer operation. A tree-based search method was employed to obtain optimal control actions from discrete switching events. To circumvent tree-based search methods, [11, 12] employed trajectory sensitivities to develop MPC strategies. However, those methods focused on voltage stability and did not take into account energy storage nor thermal overloads of transmission lines. Distributed forms of MPC have also been proposed, with mitigation of line-outage cascades considered in [13].

The authors in [14, 15] proposed a framework for electrothermal coordination in power systems, and developed temperature-based predictive algorithms that are amenable to energy markets and applicable within existing system controls. Other recent literature, cf. [16, 17], focused on model-predictive control of electrical energy systems to alleviate line overloads within a standard DC power flow framework. Specifically, the authors in [17]

4

extended the ideas of [16] to include a linearized current-based thermodynamical model of conductors and an auto-regressive model of the weather conditions (i.e. wind speed and ambient temperature) near transmission lines. This allowed [17] to set a hard upper limit on conductor temperature to ensure control objectives, and allowed MPC to operate the system closer to actual physical limits than if using standard (worst-case weather-based) thermal ratings. Furthermore, [17] illustrated that temperature-based control can outperform current control within a predictive framework.

The cascade-mitigation scheme described in this chapter is motivated by the bilevel control structure that was introduced in [18] for large-scale energy-hub systems and considers both the economic and static security objectives in operation of the system. The first level operates on a slow timescale (i.e. hourly) and determines a trajectory of optimal economical set points for generation, storage, load control, and wind curtailment. The second level responds to contingencies (i.e. line outages) on a much faster minute-by-minute timescale to ensure that the system is driven back to a secure operating regime and line overloads are alleviated. The second level does not consider fault conditions and automatic protection schemes, which operate on a sub-second timescale, and assumes transient short-term stability. A temperature-based cascade mitigation is described for the electric bulk power system where the role of energy storage is highlighted. The work herein represents state of the art in model-predictive cascade mitigation.

3.3. Chapter Outline

The chapter is organized as follows. First, basic relevant concepts are described, including line outage models. Then, relevant system models are introduced and the use of MPC is motivated for cascade mitigation. A bi-level cascade mitigation scheme that considers economic and security objectives is then discussed. A cascade mitigation approach that utilizes model-predictive control (MPC) is discussed and focuses on receding-horizon MPC of electric bulk power systems with energy storage. Analysis of the feedback scheme is provided. The receding-horizon MPC scheme is complemented with a case-study of the standard IEEE RTS-96 test system augmented with energy storage to highlight the practical, yet rigorously justified, cascade mitigation scheme.

4. Basic concepts and definitions

To ameliorate possible confusion with terminology, relevant definitions and concepts are described in this section.

4.1. Line tripping

When lines exceed their limits, it is possible that these lines go out of service or trip. The term "line trip" refers to the event that causes a line to go from being in-service to out-of-service. When a line (i, j) is tripped (i.e. out of service) the following must hold:

- no flow (or losses) across (i, j): $f_{ij} = 0$.

- node i and j are decoupled in power flow equations. For example, the DC power flow equation, $x_{ij} f_{ij} = \theta_i - \theta_j$, that relates the voltage phase angles of nodes i and j to flow across line (i, j) no longer has to hold.

In general, one of the main goals of a system operator is to ensure that line flows stay within predefined flow limits, which represents a form of network reliability. Therefore, if $f_{ij}(t)$ and u_{ij} are the (bidirectional) power flow and the power flow rating (i.e. limit) on arc (i, j) at time t, respectively, then, it is desirable to enforce the line flow limit:

$$|f_{ij}(t)| \leqslant u_{ij}, \tag{1}$$

where (i, j) represents arc between nodes i and j. Thus, if system operations satisfy (1) at all times t, arc (i, j) will not be tripped (under normal operating circumstances).

While it is feasible to take inequality (1) into consideration upon determination of an hourly economic energy management schedule, it is unrealistic to expect such a constraint to be valid after the system undergoes a significant disturbance (e.g. multi-line outage). This is due to the fact that flows depend on the physics of the network and cannot be directly guided (e.g. FACTS devices[1] are not considered here), which means that the line flows may exceed their limit after a contingency has occurred.

---

[1]Flexible AC Transmission System (FACTS) devices employ power electronics to control AC system parameters, such as impedance, which enables some controllability of line flows.

There exists a myriad of approaches to model when overloaded line should be tripped, ranging from deterministic hard constraints, as in [19], to soft-constrained probabilistic setups described in [20]. This chapter employs a probabilistic line-outage model based on temperature overloads.

4.1.1. Probabilistic Thermal Outage Model

The probabilistic model of line tripping is utilized in Section 7 to appropriately represent the actual line outage process for electrical transmission systems. For electrical systems, components, such as over-current relays, are often in place to protect the system against abnormal conditions by tripping lines (i.e. taking them out of service). However, these components operate for extreme over-current fault scenarios (e.g. 10 000 A) and trigger automatically on a timescale of seconds and mili-seconds and are, therefore, not considered in this work. Instead, the line-tripping behavior of interest in this chapter occurs on a timescale of minutes, which shifts the focus from fault-conditions to thermal conditions of transmission lines and sagging. Electrical transmission lines have prescribed power flow limits to prevent dangerous sagging and permanent damage. These limits are related to the thermal capacity of the conductor and the current flowing across the line. The method for calculating the current-temperature relationship of bare overhead transmission lines is described in detail by IEEE Standard 738 [21]. As the temperature of the conductor increases, the thermal expansion causes the line to sag. There is an inverse relationship between the overload on a line and the time it takes before the line sags excessively and must be taken out of service; however, there are no clear rules when a sagging line will be taken out of service (by operator or nature). For example, a human system operator may decide that the red flashing warning sign is sufficiently annoying and trip the line manually or an elephant may just walk into a sufficiently sagging line and cause an outage[2]. Excessive line temperature (and resulting sag or possible annealing) may eventuate in line-tripping. In short: *the higher the temperature, the more likely line tripping becomes.* This inverse relationship between conductor temperature and mean time-to-trip (i.e. mean time-to-failure) is captured in the actual system by use of the exponential time-to-failure den-

---

[2]This has actually happened more than 120 times in India since 2000 [22].
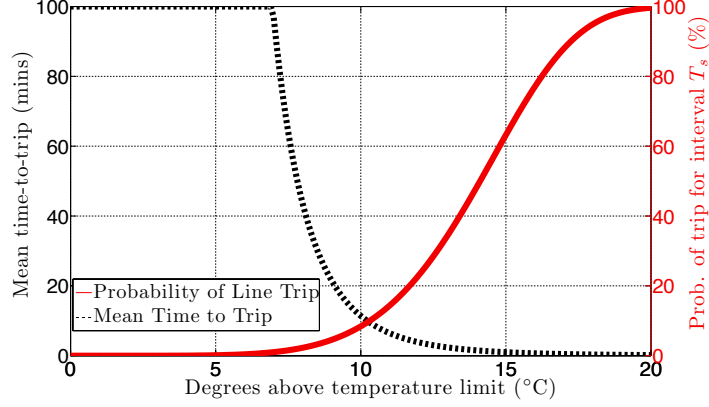
Figure 2: Probabilistic line outage model based on exponential time-to-trip distribution with $\lambda(\Delta T_{ij}[k]) = (\Delta T_{ij}[k]/15)^6$ from STE overload temperature rating. Tripping times beyond 100 minutes have been truncated for graphical purposes.

sity parametrized by the temperature overload:

$$P\left(\text{line } (i,j) \text{ trips at time } t\right) = \lambda(\Delta T_{ij})e^{-\lambda(\Delta T_{ij})\,t}, \tag{2}$$

where rate parameter $\lambda(\Delta T_{ij}) > 0$ is a nonlinear function of the temperature overload, defined such that the mean time-to-failure goes to zeros as temperature increases (i.e. $\frac{1}{\lambda(\Delta T_{ij})} \to 0$ as $\Delta T_{ij} \to \infty$). That is, for each temperature overload, there is different mean time-to-failure. Thus, the probability of line (i,j) tripping during time-interval T_s, given ΔT_{ij}, is defined by the cumulative density function (also called the *unreliability function*):

$$P\left(\text{line } (i,j) \text{ trips during time } k\,|\,\Delta T_{ij}[k]\right) = 1 - e^{-\lambda(\Delta T_{ij}[k])\,T_s}, \tag{3}$$

where rate parameter $\lambda(\Delta T[k]) > 0$ can be based on the short-time (15-minute) emergency (STE) rating of a transmission line. It has been found experimentally that $\lambda(\Delta T_{ij}[k]) = (\Delta T_{ij}[k]/15)^6$ gives reasonable line tripping behavior, as shown in Fig. 2. Notice how the mean time-to-trip decreases with increasing conductor temperature overload.

Furthermore, considering over-current protection on transmission lines (for large overloads), an additional condition can be added to the probabilistic

8

line-tripping model:

$$P\left((i,j) \text{ trips at } k \,\middle|\, \frac{|f_{ij}^{ac}[k]|}{u_{ij}} \geqslant \overline{\Omega}\right) = 1, \qquad (4)$$

where $\overline{\Omega}$ is an upper bound on allowable relative *instantaneous* overload. For example, if $\overline{\Omega} = 3$, then a line flow of 300% of nominal thermal limit u_{ij} automatically trips line (i,j).

With this formulation for line-tripping, if a line experiences an overload, the expected time to trip decreases as a function of the inverse of temperature-based rate-parameter $\lambda(\Delta T_{ij})$ and sampling time T_s.

Remark 1. (Implementation of line-tripping) If line switching is an admissible action of the controller, a mixed-integer disjunctive line outage can be employed [18, 23]. However, to be clear, line tripping is not considered as a decision available to the controller. That is, it is assumed that network topology is observable at all times and that line outages are known to the controller immediately after they occur, which means that line outages only represent a exogenous input for the system (i.e. a disturbance).

4.2. Cascade failures

Given a line-outage model, we can discuss cascade failures. From left to right, Fig. 3 illustrates three stages of a cascading failure: initial disturbance (left side of figure), cycles of line outages and flow redistributions (center), and a terminal blackout (right). Cascade failures are initiated when a disturbance occurs that forces a redistribution of flows. When a line goes out of service, it can reduce the network's overall capacity[3], which begets power overloads on the remaining lines as the power flows are redistributed according to Kirchhoff's laws. If overloads are not alleviated in a timely manner, more lines may go out of service. The cycle of line outages and redistribution of flows, if left uncontrolled, is referred to as a cascade failure. A cascade failure generally terminates in a major blackout, with large areas of a network unable to supply demand.

---

[3]The Braess Paradox [24] states that adding capacity to networks can, in some instances, actually increase congestion. Conversely, removing capacity (i.e. lines) does not guarantee an increase in grid congestion, overloads, and cascade failures, see [19] for example networks.
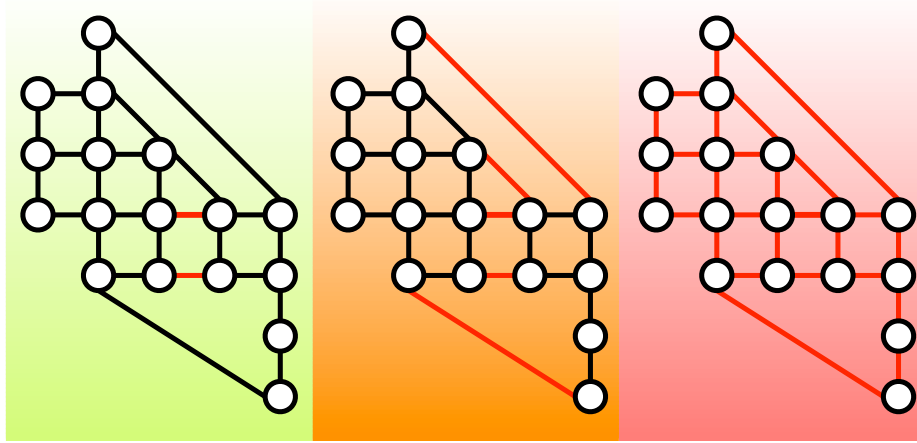
Figure 3: From left to right, illustration of the general process of a cascade failure in a network: initial disturbance, overloads and line tripping, and terminal blackout.

Furthermore, for electric power grids, the cascade is multi-scale in a somewhat unusual way. After the initial fault, the first stages of grid failure can proceed relatively slowly, on a scale of hours or minutes. As the cascade develops, the pace of failures can accelerate, with later waves happening on a scale of seconds. Fig. 4 highlights the accelerating pace of major outage events during the 2003 blackout in Northeastern US and Canada. Note that the initial two outage events represent transmission lines overheating and sagging into trees, which is exactly the focus of this chapter. The multi-scale timing of outages has important consequences for any cascade-mitigation strategies. Since longer time scales during the initial cascade allow for significant computations to be performed, it provides an excellent opportunity for feedback control in mitigating the effect of cascading failures. This provides the motivation for the model-predictive control approach developed in later sections.

5. System considerations

The cascade-mitigation schemes proposed herein rely on successive solutions to large optimization problems that drive the system back to a safe and economical operating regime. Large optimization problems generally produce numerical problems for solvers or simply take too long to solve to optimality. Therefore, it is crucial that the cascade-mitigation schemes employ models
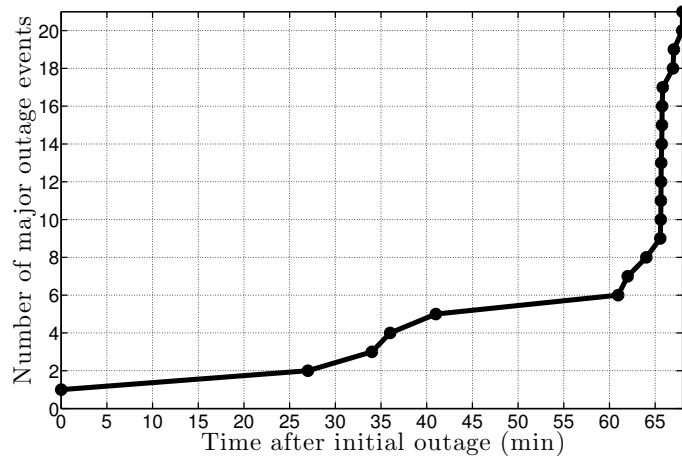
Figure 4: Visualizing the evolution of the August 2003 blackout in Northeastern US and Canada. Data is taken from description of different outage phases in [6].

that are amenable to fast and robust computation. To that effect, we have taken the technical route of employing strictly linear (i.e. convex) models. They are described in the following sections.

5.1. Multi-energy concept: the energy hub

Multi-carrier energy networks may be formulated in different ways. This section will focus the discussion on the "hybrid energy hub" model initially developed by [25]. Under this formulation, the system operator of an energy hub network can directly manipulate and control load, generator, and energy hub (e.g. storage and converter) set points. The energy hub model is linear, which makes it amenable for computation and optimization. For mathematical details on the energy hub models, please see [26].

Most common energy hubs consist of five simple interconnected elements: inputs, input-side energy storage, energy converters, output-side energy storage, and outputs. To properly describe the flow of power through the energy hub, we need to describe how power flows between these elements. Energy carrier networks supply power to the hub at the input side, where storage may be available. The energy that was not utilized for storage is dispatched into converters that transform the energy accordingly. On the output side of the hub, converted energy may be utilized for storage or injected into the carrier network connected to that side.

One simple example of an energy hub is shown in Fig. 5 where a cam-
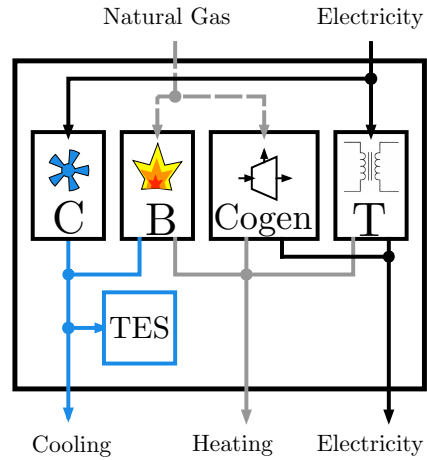
11

Figure 5: Simple illustration of a multi-energy campus energy plant as an energy hub.

pus energy plant is modeled as an energy hub. The chilled water plant (C), natural-gas steam boiler plant (B), gas turbine cogeneration plant (Cogen), electrical substation (T), and thermal energy storage (TES) are considered part of the the same energy hub. The supply of electricity and natural gas represent the hub inputs while the outputs are cooling, heating, and electric loads (e.g. buildings and/or processes). The electrical energy is converted to cooling via the chilled water plant and to low-voltage electrical energy by the transformer at relevant efficiencies and injected into the output side. The natural gas consumed at the hub input can be dispatched to the steam boilers (for heating only) or to the Cogen plant where natural gas is converted into both electrical energy and heating. To illustrate the inclusion of storage devices within the energy hub formulation, consider the chilled water storage tanks in TES that can store cooling at some charge/discharge efficiency and standby losses. The chilled water plant can store cooling from the electric chillers while the boiler plant can store cooling via absorption processes. The TES can then charge or discharge to achieve objectives related to improved economics (e.g. reduce peak electric consumption) and/or increased reliability (e.g. provide backup when chilled water plant is out of service).

5.2. Energy hubs and cascade mitigation

As was illustrated in our initial work on cascade mitigation, please see [27], energy hub storage can play a significant role in cascade mitigation since it

12

acts as a "buffer" against disturbances. That is, a system operator can employ stored energy to satisfy temporary energy shortages or overflows, while allowing time for conventional generators to effectively reconfigure their schedules. Thus, the effectiveness of system operations in minimizing costs and rejecting disturbances depends on the available energy storage infrastructure. Indeed, siting, sizing, and operational capability (e.g. power rating and standing losses) are salient parameters. Siting is important for reducing congestion during peak hours; however, the process for determining optimal location of energy storage is non-trivial and is not considered.

In [27], it was shown through simulations the effects of varying storage capacity and charge/discharge power limits on the cascade mitigation process. Under the energy hub paradigm, we were able to combine multiple types of energy systems and study their combined performance. Therefore, we needed to consider multiple types of energy storage, namely, natural gas storage, electrical storage, and thermal storage. The energy-hub scheme developed in [27], illustrates the active role of energy storage and conversion processes and the ability of a bilevel scheme to balance both economic and security objectives in the cascade mitigation scheme. It is shown that energy resources must be carefully regulated because MPC has a tendency to over-exploit stored energy to the detriment of long-term energy requirements.

Note that this chapter significantly extends the work presented in [27] and focusses on the electric transmission system and associated energy storage devices. Furthermore, we consider energy storage to have no standing losses, constant charging and discharging efficiencies, and we neglect the economics of construction, operation, and maintenance of storage facilities. That is, energy storage represents a cost-free service available to the system operator.

5.3. Energy Storage Model

The systems considered in this chapter will have energy storage located at various nodes throughout the network. During normal operation of the power system, energy storage plays a significant role in minimizing generation costs from conventional generators, as it allows the system operator to pre-position energy in storage during off-peak hours to satisfy demand in the presence of intermittent generation (e.g. wind power) or take advantage of arbitrage. However, during contingency operation, economics become a secondary concern, but energy storage can still play a significant role in cascade mitigation as it acts as a "buffer" against disturbances. That is, a system operator can employ stored energy to satisfy temporary energy

shortages or overflows, while allowing time for conventional generators to effectively reconfigure their schedules against ramp-rate limits.

Energy storage is available in many forms (e.g. hydrogen fuel cells, grid-scale battery systems, pumped hydro, thermal energy storage, etc) and energy storage devices can be located at various nodes throughout a network. Let $n \in \Omega_i^E \subset \mathcal{Q}$ be an energy storage device at node i, where $\mathcal{Q}$ is the set of storage devices in the system. Assume steady-state storage power values, a constant slope for $\dot{E}_n(t) = dE_n(t)/dt$, and treat storage interface as a conversion process with charging and discharging efficiencies $\eta_{c,n}$ and $\eta_{d,n}$, then the relationship between storage state-of-charge (SOC) and power injected/consumed by device n is

$$\dot{E}_n(t) = \frac{dE_n(t)}{dt} \approx e_n(t, f_{Qn}) \times f_{Qn}(t). \tag{5}$$

where the SOC switching mechanism e_n is defined as

$$e_n(t, f_{Qn}) = \left\{ \begin{array}{ll} \eta_{c,n}, & \text{if } f_{Qn}(t) \geqslant 0 \quad \text{(charge/standby)} \\ \frac{1}{\eta_{d,n}}, & \text{if } f_{Qn}(t) < 0 \quad \text{(discharge)} \end{array} \right. . \tag{6}$$

Since energy storage devices have two distinct states of operation, charging and discharging, that achieve different efficiencies, energy storage devices introduce switches in the SOC formulation. The following reformulation of the SOC makes this non-convex nonlinearity more apparent:

$$\dot{E}_n(t) = \eta_{c,n} f_{Qc,n}(t) + \frac{1}{\eta_{d,n}} f_{Qd,n}(t) \tag{7a}$$

$$f_{Qn}(t) = f_{Qc,n}(t) + f_{Qd,n}(t), \tag{7b}$$

$$0 = f_{Qc,n}(t) f_{Qd,n}(t) \tag{7c}$$

where the rate-limited charging (c) and discharging variables (d), $f_{Qc,n} \in [0, \overline{f}_{Qc,n}]$ and $f_{Qd,n} \in [-\overline{f}_{Qd,n}, 0]$, model the switching mechanism explicitly as a complimentarity condition in (7c). The nonlinear complimentarity condition ensures that q can either charge or discharge, but not both simultaneously. To circumvent the nonlinearity, a mixed-integer linear (MIL)

14

formulation can be employed:

$$\textbf{MIL:} \ f_{Qc,n}(t)f_{Qd,n}(t) = 0 \iff \begin{cases} 0 \leqslant f_{Qc,n} \leqslant \overline{f}_{Qc,n}(1 - z_n) \\ -\overline{f}_{Qd,n}z_n \leqslant f_{Qd,n} \leqslant 0 \\ z_n \in \{0, 1\} \end{cases}. \quad (8)$$

where z_n is a binary integer. For example, if $z_n[k] = 1$, then $f_{Qc,n}[k] \equiv 0$ and device n is consequently operating in discharging mode at time-step k. While the above linear formulation is equivalent to the nonlinear complimentarity condition, the use of integers is generally not desired, as it greatly increases computational complexity.

To avoid utilizing integers in the linear model, one can ignore the complimentary condition in (7c). This implies that simultaneous charging and discharging is now mathematically feasible and is equivalent to a convex relaxation of the original SOC model. Replace (7) with the strictly linear and continuous formulation:

$$\dot{E}_n(t) = \eta_{c,n} f_{Qc,n}(t) + \frac{1}{\eta_{d,n}} f_{Qd,n}(t), \quad (9a)$$

$$f_{Qn}(t) = f_{Qc,n}(t) + f_{Qd,n}(t). \quad (9b)$$

Employing a Forward Euler Discretization to (9) with sample-time of T_s seconds admits linear continuous first-order discrete SOC dynamics that represents the full linear energy storage model:

$$E_n[k + 1] = E_n[k] + T_s \eta_{c,n} f_{Qc,n}[k] + \frac{T_s}{\eta_{d,n}} f_{Qd,n}[k] \quad (10a)$$

$$f_{Qn}[k] = f_{Qc,n}[k] + f_{Qd,n}[k] \quad (10b)$$

$$f_{Qc,n}[k] \in [0, \overline{f}_{Qc,n}], \ f_{Qd,n}[k] \in [-\overline{f}_{Qd,n}, 0]. \quad (10c)$$

Remark 2. The MIL formulation of (8) was implemented in [27] to model non-simultaneous charging and discharging for energy hubs. However, for systems with a large number of storage devices, due to the complexity of integer optimization in the MIL approach, the MIL model is abandoned in Section 7 and replaced by the strictly continuous linear convex approximation (10). The effects of allowing simultaneous charging and discharging (i.e. *"simul-charge"*) is discussed then and a suitable heuristic is introduced that reduces the unwanted effects of simul-charge.

15

5.4. Power flows

Energy hubs are interconnected via multiple energy supply networks. The previous section defined how power flows through an energy hub, however, to describe the flow between energy hubs, we need to consider power networks. A power network is a collection of a set of nodes $i \in \mathcal{N}$ (e.g. buses) and a set of arcs $(i, j) \in \mathcal{A}$ (e.g. transmission lines and gas pipelines) that define a simple graph, as shown in Fig. 6. The nodes either consume power from the network (i.e. loads), inject power into the network (i.e. generators), or act as throughput nodes that neither inject nor consume power. The sum of power flows into the network (e.g. hub outputs, generators) must equal the sum of flows out of the network (e.g. hub inputs, loads, and losses). In fact, any network must satisfy Kirchhoff's First Law (also called the "power balance"). That is, the net flow into a node must equal the net flow out of the node. Generally, a node may have generators (f_{Gn}) and/or loads (f_{Dn}) available and, in a system with energy storage devices, the charging (discharging) corresponds to additional demands (injections) (f_{Qn}). Therefore, the power balance equation is formulated as:

$$\sum_{n\in\Omega_i^D} f_{Dn}[k] - \sum_{n\in\Omega_i^G} f_{Gn}[k] + \sum_{j\in\Omega_i^N} f_{ij}^{\text{total}}[k] + \sum_{n\in\Omega_i^E} f_{Qn}[k] = 0 \quad \forall i \in \mathcal{N} \quad (11)$$

where $f_{ij}^{\text{total}} = f_{ij} + \frac{1}{2} f_{ij}^{\text{loss}}$ is the total flow across line (i, j) and

- Ω_i^G – set of generators at node i (hub outputs and conventional)

- Ω_i^N – set of nodes adjacent to node i

- Ω_i^D – set of demands (loads and hub inputs) at node i

- Ω_i^E – set of energy storage devices at node i.

The power balance equation in (11) determines the net power generated or consumed at each node. As well as contributing to the power balance, line losses f_{ij}^{loss} also drive the temperature dynamics associated with line overloads. This dual role will be carefully studied in Section 7.

Besides interconnecting energy hubs, the main difference between a simple graph and a power network lies with the physics of the particular power flows. That is, there exists a physical relationship between the flow across an arc
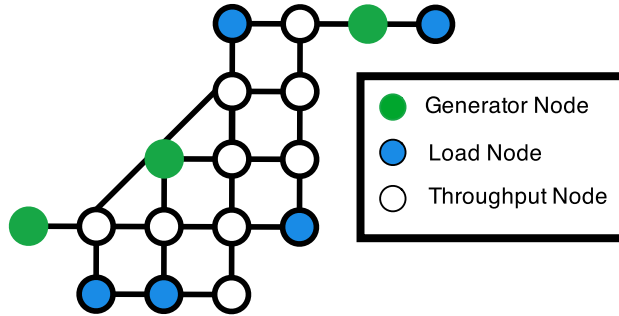
16

Figure 6: Representation of a power network as a graph.

and the connected nodes. For a simple example, consider an electrical power network and the linear DC flow model:

$$x_{ij}f_{ij} = \theta_{ij} \tag{12}$$

where x_{ij} represents the reactance of arc (i,j), f_{ij} is the power flow across said arc, and $\theta_{ij} := \theta_i - \theta_j$ represents the voltage phase angle difference between nodes i and j. In (12), we see that the electrical power flowing across any arc depends on the difference in the phase angle between connected nodes and the reactance of the arc. This physical relationship between nodes and arcs manifests itself differently depending on the nature of the power network model and may be linear (e.g. DC power flow) or nonlinear (e.g. AC power flow). Regardless of the type of power network, a set of equations describing the appropriate power flow and power balance can be formulated. In this work, the cascade-mitigation schemes employ a linear model of power flows (i.e. a DC power flow) in the controller. The simulation results will illustrate the value of such simplified controller models for cascade mitigation on AC networks.

5.5. Transmission Line Losses

The probabilistic temperature-based line outage model described in Section 4.1.1 requires consideration of conductor temperature, which depends on ohmic I^2R losses, local ambient conditions (wind speed, insolation), and conductive and radiative conductor heat losses. Thus, to alleviate temperature overloads caused by ohmic heating in transmission lines, it is necessary for a controller to model and manipulate I^2R line losses. However, the DC power flow model in (12) ignores active line losses. To establish a relationship

17

for losses on branch (i, j), the AC expression for active power flow across a transmission line can be manipulated to give:

$$f_{ij}^{\text{loss}} = f_{ij} + f_{ji} = g_{ij} \left(U_i^2 + U_j^2 - 2\, U_i U_j \cos \theta_{ij} \right). \tag{13}$$

where g_{ij}, U_i, θ_{ij} are line's (i, j) conductance, nodal voltage magnitude, and voltage phase angle difference, respectively. Assuming voltage magnitudes are close to 1.0 pu and approximating $\cos \theta_{ij}$ by a second-order Taylor series expansion gives,

$$f_{ij}^{\text{loss}} \approx 2g_{ij} \left(1 - \cos \theta_{ij} \right) \approx g_{ij} \theta_{ij}^2. \tag{14}$$

$$\Rightarrow f_{ij}^{\text{loss}} \approx \frac{r_{ij}}{r_{ij}^2 + x_{ij}^2}\, \theta_{ij}^2 \approx \frac{r_{ij}}{x_{ij}^2}\, \theta_{ij}^2, \tag{15}$$

where the final step follows because $x_{ij} \geqslant 4r_{ij}$ for most transmission lines. Thus, the "DC" line losses can be written as follows:

$$f_{ij}^{\text{loss}} \approx \frac{r_{ij} \theta_{ij}^2}{x_{ij}^2} = r_{ij} f_{ij}^2, \tag{16}$$

with the DC flow f_{ij} defined in (12). Note that the loss term f_{ij}^{loss} is quadratic in θ_{ij} and is therefore not suitable for a strictly linear constraint formulation.

A computationally amenable model of the quadratic losses can be incorporated into a linear optimization formulation by applying a (piece-wise) linear approximation of losses that circumvents the need for integer optimization, see [28, 29, 30]: PWL[f_{ij}^{loss}]. In fact, you can employ PWL[.] to line losses and develop a strictly (piece-wise) linear model of active line losses
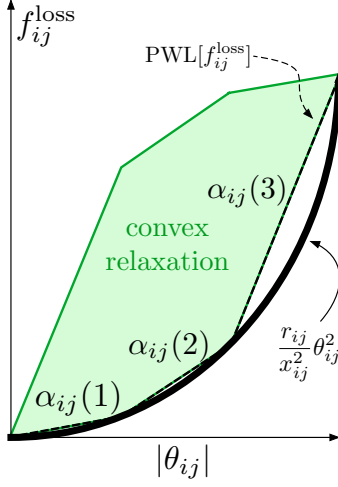
18

Figure 7: PWL convex relaxation of line losses for PWL approximation with $S = 3$.

in (16) with the following relations:

$$f_{ij}^{\text{loss}} := \frac{r_{ij}}{x_{ij}^2} \Delta\theta \sum_{s=1}^{S} (2s-1)\theta_{ij}^{\text{PW}}(s) \tag{17a}$$

$$\sum_{s=1}^{S} \theta_{ij}^{\text{PW}}(s) = \theta_{ij}^+ + \theta_{ij}^- \tag{17b}$$

$$\theta_{ij} = \theta_{ij}^+ - \theta_{ij}^- \tag{17c}$$

$$\theta_{ij} \in (-\theta_{\max}, \theta_{\max}) \tag{17d}$$

$$0 \leqslant \theta_{ij}^+, \theta_{ij}^- \tag{17e}$$

$$\theta_{ij}^{\text{PW}}(s) \in [0, \Delta\theta]. \tag{17f}$$

The linear constraint formulation presented in (17) is, in fact, a convex relaxation of the "DC" line losses. Figure 7 illustrates the relaxation of PWL line losses. Note that the relaxation given by (17) yields a value for f_{ij}^{loss} that is greater than or equal to the piece-wise linear approximation $\text{PWL}[f_{ij}^{\text{loss}}]$. Equality occurs only when both $|\theta_{ij}| \equiv \theta_{ij}^+ + \theta_{ij}^-$ and $\theta_{ij}^{\text{PW}}(s) > 0 \Rightarrow \theta_{ij}^{\text{PW}}(n) = \Delta\theta, \forall n < s$ (i.e. PWL adjacency conditions). Under such conditions, the relaxation is considered "tight" and the model is exact with respect to PWL, and the convex relaxation of line losses provides a more accurate method for estimating line losses than standard linearization. When the losses are

19

relaxed (i.e. not tight), overestimated losses are denoted "fictitious losses", as they exist only as an artifact of the MPC controller model and not in the actual system.

5.6. Model-predictive control

Literature provides two generic approaches for mitigating cascade failures in power networks. The first method predicts disturbances *a priori* and is based on an off-line computation of all possible or likely failures in the network — the so-called $N - k$ problem, e.g. [31]. With such an approach, control policies are devised to deal with each possible disturbance. A major drawback of this approach is that it does not scale well, since the number of salient contingencies to consider increases exponentially with network size. A second method is based on retroactive control, whereby the uncertainty surrounding the disturbance has been revealed and one can utilize the knowledge available about the disturbance to determine control responses in real-time to mitigate the effects of the disturbance. In the latter approach, the multi-timescale nature of cascading failures provides sufficient time for post-contingency computations. In addition, power/energy systems are suffused with constraints on control inputs and states, which makes model predictive control (MPC) particularly useful in a cascade-mitigation scheme.

MPC is an advanced method of process/batch control that has gained prominence over the last 30 years from its extensive deployment in the chemical industry. For a thorough technical discussion of predictive control in linear systems, please see [8]. Basically, MPC provides a method for controlling dynamic systems with constraints on inputs and/or states using tools from optimization. MPC implementations solve on-line, at each sampling instant, a finite horizon optimal control problem based on a dynamic model of the plant. Most MPC approaches can be described by the following algorithm:

1. Determine a control sequence that optimizes an objective function over a prediction window, where the measured or estimated state at time-step k is the initial state.
2. Apply the computed control profile until new process measurements become available,
3. When new measurements are available, set $k = k + 1$ and repeat step 1.

MPC is most often formulated in the state space by linear discrete-time difference equations. The mathematical formulation is given below.

20

MPC Formulation The objective of MPC is to drive the system from it's current state to some reference state, given by a set-point, x^{sp}, in the "best possible" way. Power systems are often modeled with a mix of differential and algebraic states, which beget a set of differential-algebraic equations (i.e. equality constraints). In this work, the constraints are assumed linear (i.e. nonlinear MPC is not discussed) and an l_2-norm describes the objective function, therefore, MPC can be formulated as a quadratic programming (QP) problem over a finite prediction horizon[4] of length M:

$$U^*[k] = \min_{u[l|k]} \left\| x[M|k] - x^{\text{sp}}_{k+M} \right\|_{S_M} + \sum_{l=0}^{M-1} L\left(x[l|k], u[l|k] \right) \tag{18a}$$

$$\text{s.t.} \quad x[l+1|k] = Ax[l|k] + Bu[l|k] + Fz[l|k] \tag{18b}$$

$$0 = \hat{A}x[l|k] + \hat{B}u[l|k] + \hat{F}z[l|k] \tag{18c}$$

$$Cx[l|k] + Du[l|k] + Gz[l|k] \leqslant d \tag{18d}$$

$$x[l|k] \in \mathcal{X}, \, u[l|k] \in \mathcal{U}, z[l|k] \in \mathcal{Z} \tag{18e}$$

$$x[M|k] \in \mathcal{T}_x \tag{18f}$$

$$x[0|k] = x^{\text{meas}}_k \tag{18g}$$

where $x[l|k]$, $u[l|k]$, and $z[l|k]$ represent the dynamic state, control input, and algebraic state variables, respectively, at predicted time $0 \leqslant l < M$, given initial measured state x^{meas}_k at time k. The optimizer,

$$U^*[k] = \{u^*[0|k], u^*[1|k], \ldots, u^*[M-1|k]\}, \tag{19}$$

represents the open-loop optimal control sequence over the prediction horizon at time k. The appropriately-sized matrices A, B, F and $\hat{A}, \hat{B}, \hat{F}, C, D, G$ describe dynamic and algebraic constraints, respectively. The objective function in (18a) is defined by:

$$L(x[l|k], u[l|k]) = ||x[l|k] - x^{\text{sp}}_{k+l}||_Q + ||u[l|k] - u^{\text{sp}}_{k+l}||_R \tag{20}$$

where x^{sp}_{k+l} and u^{sp}_{k+l} refer to a reference trajectory at time $k + l$, the

---

[4]Even though the work presented herein uses identical prediction and control horizons (i.e., $M_p = M = M_c$), it is straight-forward to consider the effect of varying either horizon, provided $M_c \leqslant M_p$

norms are defined by $||y||_B \equiv y^\top By$, and weighting matrices $S_M \succeq 0$ and $Q \succeq 0$ are non-negative definite while $R \succ 0$ is positive definite. Expressions (18b) and (18c) describe the differential-algebraic (DAE) dynamics. Expressions (18d), (18e), and (18f) define static inequality constraints, bounds on states and inputs, and a terminal state constraint set, respectively. Equation (18g) establishes the initial state for MPC.

In this chapter, one specific MPC technique is employed: receding horizon MPC[5]. The approach is described in detail within the context of cascade mitigation in Section 7.

6. Bilevel Cascade Mitigation Framework

Economic dispatch problems allow computation of economically optimal trajectories, which the system operator tracks via available generation, forecasted load, and other available control actions. However, if a significant disturbance takes place, the operator must modify his economical trajectory to prevent overloads and subsequent line outages. This requires the formulation of a contingency (safety) controller, which responds quickly to a disturbance and drives the system back to a secure and economical state, from which economic dispatch can be re-initiated and normal (economic) operation can resume. Since economic and security objectives are often competing objectives, it is natural to form two separate controllers for each task. Therefore, a bilevel hierarchical control strategy is employed. Fig. 8 illustrates the proposed bilevel operation of the system.

The "Level 1" controller is enlisted to compute an economically optimal schedule for each hour of the day. When a disturbance takes place (e.g. line outage), Level 1 provides an economic reference for the "Level 2" contingency controller, which shifts operation from economically optimal (e.g. hourly) to corrective (e.g. minute-by-minute) in order to alleviate line overloads. When Level 2 signals that the system is secure, economic operation resumes with Level 1. The Level 2 cascade-mitigation controller is formulated as an MPC problem.

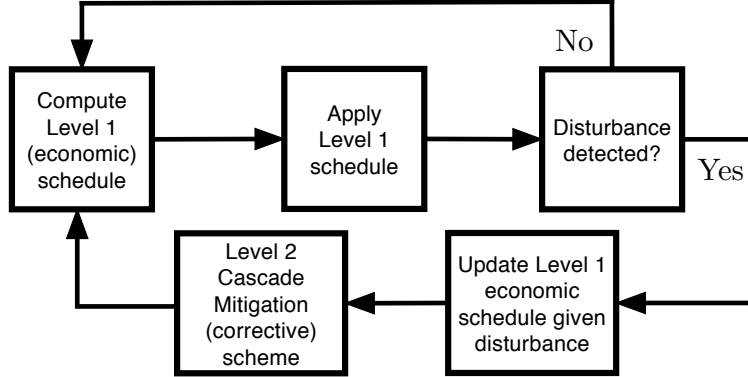[5]Another MPC technique: shrinking horizon MPC was explored in [27]

Figure 8: Overview of proposed bilevel cascade mitigation scheme.

6.1. Level 1: economically optimal energy schedule

Over a 24-hour period, Level 1 computes an optimal energy schedule that determines how to best operate energy storage, conventional generation, flexible loads, and available renewable energy based on forecasts. The Level 1 schedule is, therefore, similar to standard economic dispatch [32], except that the temporal coupling introduced by energy storage implies optimization over a horizon rather than a single time-step. In addition, any quadratic line losses can be included with a standard piece-wise linear (PWL) DC approximation as presented in [28].

The Level 1 model enforces line flow limits to ensure that, under accurate model and forecast scenarios, no lines are overloaded (i.e. the system is "safe" and economical). The dispatch schedule is computed as a multi-period quadratic programming (QP) problem whose objective is to minimize energy (fuel) costs of conventional generators:

$$\text{Cost}\,(f_{Gn}[\,k\,]) = a_n(f_{Gn}[k])^2 + b_n f_{Gn}[k]. \tag{21}$$

where a_n [\$/h-pu^2] and b_n[\$/h-pu] are constant parameters for generator n and $f_{Gn}[k]$ is its output power at time-step k.

The Level 1 schedule establishes a reference signal over a multi-hour horizon, consisting of the economically optimal system set-points x^{sp}, and the operator control actions u^{sp} required to achieve those optimal set-points. The schedule is submitted to the operator and recomputed every hour. For details on Level 1 formulation, please see [18, 26].

6.2. Level 2: corrective controller

The Level 2 controller operates in the background to track the reference trajectories computed from Level 1 (i.e. the economic set-point values). The corrective controller employs a linear model of the actual system and operates on a minute-by-minute timescale[6]. If a disturbance takes place (e.g. a line outage), Level 2 computes corrective control actions $u[k]$ in a MPC fashion that steers the system towards a safe and economically optimal state as provided by a Level 1 reference.

Level 2 considers ramp-rate limits on conventional generators, dynamics and power ratings of grid storage devices, and can incorporate the thermal response of overloaded lines. Note that, in Level 2, lines are no longer subject to a hard flow limit constraint and, instead, the controller seeks to drive overloaded lines below respective limits. The Level 2 MPC-based cascade mitigation scheme is formulated as a quadratic programming problem (QP) over a finite prediction horizon M.

In Section 7, receding-horizon MPC (i.e. M fixed) is described for a temperature-based cascade-mitigation scheme within a bulk electric power system setting.

---

[6]The Level 2 time-step T_s is much shorter than the time-step used for the Level 1 reference signals. This is resolved by linearly interpolating between reference values.

7. Cascade Mitigation in Electric Power Systems

Despite the simple energy hub formulation and the crude deterministic line overload model, the shrinking-horizon MPC scheme discussed in [27] provided valuable insight into the role of energy storage for cascade mitigation purposes and motivated the use of model-predictive control. In addition, while the coupling of energy infrastructures may provide an opportunity to improve upon network resilience and protect against cascade failure, investigations into the natural gas operations show that natural gas systems are significantly different from electric power systems. Namely, there is a timescale separation between the two power systems, with electricity flowing at nearly the speed of light while natural gas pipelines experience gas flows of up to 60 miles per hour (around 100 km/hr). This relatively slow rate of energy flowing in natural gas systems gives rise to a different role for the transmission pipeline system. Specifically, natural gas transmission systems operate by filling, *on a seasonal time-scale*, large underground natural gas storage facilities near power and heating load distribution centers. Under such physical circumstances, the notion of cascade failure in a natural gas systems becomes more of a planning problem and less of an operations problems, which reduces the value of including natural gas networks in a cascade mitigation setting. As a result, the focus in this section shifts from multi-energy system models to cascade-mitigation in bulk electric power systems where it will be shown how energy storage can be utilized to actively alleviate line overloads. In addition, the shrinking-horizon MPC and simple line-outage formulations proposed in [27] are now replaced by a more robust temperature-based formulation in the form of receding-horizon MPC. Finally, a novel energy-storage algorithm is introduced that takes advantage of the feedback inherent to MPC to overcome common challenges associated with predictive optimization of standard energy storage models.

7.1. Receding Horizon MPC

The shrinking-horizon MPC approach from [27] suffers from two major drawbacks:

- An unpredicted event could take place towards the end of the shrinking horizon period, which leaves the system unable to recover in the remaining time.

- As the horizon shrinks and approaches the final time, the control law typically "gives up trying" since there is too little time to go to achieve anything useful in terms of objective function reduction.

The above two shortcomings surrounding shrinking-horizon MPC can be overcome with the notion of *receding-horizon* MPC, which considers a prediction horizon that does not shrink but, instead, remains fixed in length and moves with time (i.e. sliding prediction window). This makes receding-horizon MPC immune against the above drawbacks and, therefore, offers a more robust control paradigm. That is, consider a system with prediction horizon of M_T minutes and sample time $T_s = 1$ minute and assume initial time-step is k, then receding-horizon MPC is summarized by the following algorithm.

Receding horizon MPC algorithm:
1. Given $x[0|k] := x[k]$, solve an optimal control problem over horizon $[k, k + M_T]$ to retrieve an open-loop control sequence $\{u[l|k]\}_{l=0}^{M_T-1}$.
2. Apply the first instance of control sequence to system: $u[k] := u[0|k]$.
3. Measure new system state $x[k + 1] := f(x[k], u[k])$.
4. Set $k = k + 1$ and repeat step (1).

As the above MPC process illustrates, with each successive control action, the horizon recedes, as the name implies. Note that in this work, the prediction and control horizons are assumed equal to M_T.

The Level 2 model for the receding-horizon MPC cascade mitigation scheme considers ramp-rate limits on conventional generators and the dynamics and power limits of grid storage devices. With the temperature-based cascade-mitigation scheme, receding-horizon MPC also incorporates the thermal response of overloaded lines. Note that in Level 2, lines are not subject to a hard flow-limit constraint. Rather, the controller seeks to drive conductor temperatures below their respective limits. Note that the receding-horizon MPC optimization is still formulated over a finite prediction horizon as described in (18).

The details of the Level 2 receding-horizon MPC model, system states, and controls are developed and discussed in [30]; however, for sake of completeness, a summary of the model is provided below. The states and inputs associated with the proposed formulation of an MPC cascade mitigation scheme for an electric power system are outlined below:

Dynamic states (x): there are three types of dynamic states:

- $\Delta \hat{T}_{ij}$, line (i,j) conductor temperature overload w.r.t. limit T_{ij}^{lim}.

- E_n, state-of-charge (SOC) for energy storage (ES) device n.

- f_{Gn}, power output level for generator n.

Control inputs (u): the formulation employs five types of control inputs:

- Δf_{Gn}, change to conventional generator n output level.

- $f_{G_W n}^{\text{spill}}$, wind spilled from nominal, for wind turbine n.

- f_{Dn}^{red}, demand response (reduction) from nominal, for load n.

- $f_{Qc,n}$, $f_{Qd,n}$, charge (c) and discharge (d) rates for ES n.

Uncontrollable inputs: there are three types of forecast (uncontrollable) inputs (i.e. exogenous disturbances):

- $f_{G_W n}^{\text{nom}}$, nominal available power from wind turbine n.

- f_{Dn}^{nom}, nominal demand, for load n.

- d_{ij}, ambient temperature and solar gain, for line (i,j).

Algebraic states (z): models require nine types of algebraic states:

- f_{ij}, real power flowing through line (i,j).

- f_{ij}^{loss}, real power losses for line (i,j).

- θ_{ij}, phase angle difference between nodes i and j.

- $\theta_{ij}^{+}, \theta_{ij}^{-}$, absolute value approximation of $|\theta_{ij}|$.

- $\{\theta_{ij}^{\text{PW}}(s)\}_{s=1}^{S}$, S-segment PWL approximation of $|\theta_{ij}|^2$.

- $f_{G_W n}$, real power injected by wind turbine n.

- f_{Dn}, real power consumed by load n.

- f_{Qn}, total power injected or consumed by ES n.

From the above descriptions, state and input vectors are defined by:

$$x = \text{col}\{\Delta \hat{T}, E, f_G\} \tag{22a}$$

$$u = \text{col}\{\Delta f_G, f_{G_W}^{\text{spill}}, f_D^{\text{red}}, f_{Qc}, f_{Qd}, \psi\} \tag{22b}$$

$$z = \text{col}\{\theta, \theta^{+}, \theta^{-}, \theta^{PW}, f, f^{\text{loss}}, f_D, f_{G_W}, f_Q\}. \tag{22c}$$

7.1.1. MPC objective function

The objective of the MPC scheme is to determine the optimal control actions that alleviate temperature overloads, $\Delta \hat{T}_{ij}$, while minimizing deviations from the economic set-points established by Level 1. Accordingly, the MPC objective function is composed of the terms:

$$
\begin{aligned}
&p_o(\Delta \hat{T}_{ij}[l])^2 && \text{- line temperature overload} \\
&p_g(f_{\mathrm{G}_g}[l] - f^{\mathrm{sp}}_{\mathrm{G}_g,k+l})^2 && \text{- deviation from reference set-point} \\
&p_r(\Delta f_{\mathrm{G}_g}[l] - \Delta f^{\mathrm{sp}}_{\mathrm{G}_g,k+l})^2 && \text{- changes in generation ramping} \\
&p_e(E_n[l] - E^{\mathrm{sp}}_{n,k+l})^2 && \text{- deviation from reference SOC} \\
&p_q(Q_n[l] - Q^{\mathrm{sp}}_{n,k+l})^2 && \text{- changes in reference dis/charging} \\
&p_s(f^{\mathrm{shed}}_{\mathrm{D}_d}[l])^2 && \text{- load control} \\
&p_w(f^{\mathrm{spill}}_{\mathrm{G,wind}}[l])^2 && \text{- wind curtailment}
\end{aligned}
$$

where reference values, denoted $(\cdot)^{\mathrm{sp}}$, refer to the economically optimal set-points computed in Level 1.

Based on the state and input definitions in (22), the following weighting matrices define the objectives of the MPC scheme:

$$
Q = \mathrm{diag}\Big\{p_o I, \frac{p_e}{10M^2}I, \frac{p_g}{10M^2}I\Big\} > 0 \tag{23a}
$$

$$
S_M = \mathrm{diag}\{p_o I, p_e I, p_g I\} > 0 \tag{23b}
$$

$$
R = \mathrm{diag}\{p_r I, p_w I, p_s I, p_q I, p_q I\} > 0 \tag{23c}
$$

where I represents identity matrices of appropriate dimensions, $p_\diamond > 0$ are weighting coefficients for states and inputs, and $\mathrm{diag}\{\cdot\}$ denotes a block-diagonal matrix. Note that the terminal cost matrix S_M is designed to penalize deviations from economical references for storage SOC and conventional generation states more severely than does the weighting matrix Q. This is because MPC does not care *how* these reference signals are tracked, only that they are being considered at the end of the horizon. The weighting matrices are used in (24a).

7.1.2. Electric system constraints

For each time k, the dynamic states x^{meas}_k are measured (or estimated) and represent the initial state of the MPC system model. Then, the full

MPC formulation is defined as a quadratic programming (QP) problem:

$$\min_{u[l]} \quad \left|\left|x[M] - x^{\text{sp}}_{k+M}\right|\right|_{S_M} + \sum_{l=0}^{M-1} L\left(x[l], u[l]\right) \tag{24a}$$

s.t.

$$\Delta T_{ij}[l+1] = \tau_{ij}\Delta T_{ij}[l] + \rho_{ij}\Delta f^{\text{loss}}_{ij}[l] + \delta_{ij}\Delta d_{ij} \tag{24b}$$

$$E_n[l+1] = E_n[l] + T_s\eta_{c,n}f_{Qc,n}[l] - \frac{T_s}{\eta_{d,n}}f_{Qd,n}[l] \tag{24c}$$

$$f_{Gn}[l+1] = f_{Gn}[l] + \Delta f_{Gn}[l] \tag{24d}$$

$$\Delta\hat{T}_{ij}[l] = \max\{\Delta T_{ij}[l], 0\} \tag{24e}$$

$$0 = f_{Qc,n}[l]\, f_{Qd,n}[l] \tag{24f}$$

$$0 = x^2_{ij}f^{\text{loss}}_{ij}[l] - \Delta\theta\sum_{s=1}^{S}(2s-1)\theta^{\text{PW}}_{ij}(s)[l] \tag{24g}$$

$$0 = \theta^+_{ij}[l] + \theta^-_{ij}[l] - \sum_{s=1}^{S}\theta^{\text{PW}}_{ij}(s)[l] \tag{24h}$$

$$0 = \theta^+_{ij}[l] - \theta^-_{ij}[l] - \theta_{ij}[l] \tag{24i}$$

$$0 = \Gamma_i\left(f_{ij}[l], f^{\text{loss,est}}_{ij,k}, f_{Gn}[l], f_{Dn}[l], f_{Qn}[l], f_{G_Wn}[l]\right) \tag{24j}$$

$$0 = x_{ij}f_{ij}[l] - \theta_{ij}[l] \tag{24k}$$

$$f_{Dn}[l] = f^{\text{nom}}_{Dn}[l] - f^{\text{red}}_{Dn}[l] \tag{24l}$$

$$f_{Qn}[l] = f_{Qc,n}[l] - f_{Qd,n}[l] \tag{24m}$$

$$f_{G_Wn}[l] = f^{\text{nom}}_{G_Wn}[l] - f^{\text{spill}}_{G_Wn}[l] \tag{24n}$$

$$x[l] \in \mathcal{X},\ u[l] \in \mathcal{U},\ z[l] \in \mathcal{Z} \tag{24o}$$

$$x[M] \in \mathcal{T}_x \tag{24p}$$

$$x[0] = x^{\text{meas}}_k \tag{24q}$$

for all $l \in \mathcal{M}$, where $x[l]$, $u[l]$, and $z[l]$ represent the dynamic state, control input, and algebraic state variables, respectively, at predicted time $k+l$ given initial measured state at time k, x^{meas}_k. This notation has been adopted for clarity of presentation. The more precise forms, $x[l|k]$, $u[l|k]$, and $z[l|k]$, appear in [30]. The objective function (24a) was described in the last section

and is defined by (20).

Expressions (24b), (24c) and (24d) represent the linear (discrete-time) dynamics associated with conductor temperature for line (i, j), SOC for energy storage device n, and the power supplied by generator n, respectively. The thermal conductor model is based on the IEEE standard describing the temperature-current relationship in overhead conductors [21]. Temperature dynamics in (24b) are linearized with respect to the conductor temperature ($T_{ij}^{\lim}$ [°C]) obtained for steady-state ampacity ($I_{ij}^{\lim}$ [A]), and conservative ambient parameters. Accordingly, $\Delta T_{ij} = T_{ij} - T_{ij}^{\lim}$ and $\Delta f_{ij}^{\text{loss}} = f_{ij}^{\text{loss}} S_b / 3L_{ij} - R_{ij}(I_{ij}^{\lim})^2$, where S_b [VA] and L_{ij} [m] are the three-phase per-unit power base and conductor length, respectively, and R_{ij} [Ω/m] is the resistance per unit length. Also, $\Delta d_{ij} = d_{ij} - d_{ij}^*$ describes deviations from representative exogenous conditions, ambient temperature T_{amb}^* and solar heat gain rate q_s^*, with q_s a function of conductor diameter and solar conditions. However, it has been assumed for these studies that ambient temperature and solar heat gain rates remain fixed over the period of interest (i.e. $\Delta d_{ij} = 0$).

Constraint (24e) enables the main objective of alleviating temperature overloads while not incentivizing under-loading of lines. That is, MPC should compute control actions that only consider lines with $\Delta T_{ij}[l] > 0$. Keeping in mind the QP formulation, the implementation of this temperature objective can be relaxed to the linear formulation:

$$0 \leqslant \Delta \hat{T}_{ij}[l] \tag{25a}$$

$$\Delta T_{ij}[l] \leqslant \Delta \hat{T}_{ij}[l]. \tag{25b}$$

Because the objective function penalizes $\Delta \hat{T}_{ij}$, this relaxation will always be tight.

The complementarity condition (24f) ensures that energy storage devices cannot simultaneously charge and discharge. Since exact (integer-based) implementation of complementarity would considerably increase computational complexity of the proposed scheme, the algorithm described in Section 7.1.4 has been adopted for (approximately) enforcing (24f).

A convex piece-wise linear (PWL) approximation of line losses is described by algebraic relations (24g), (24h), and (24i). This PWL relaxation utilizes S segments of width $\Delta \theta = \theta_{max}/S$ and is modeled using the algebraic states $\theta_{ij}^+, \theta_{ij}^-, \{\theta_{ij}^{\text{PW}}(s)\}_{s=1}^S$. In [30], it was proven that if a line experiences a tem-

perature overload at predicted time $l + 1$, then for all prior time-steps (i.e. $\kappa \leq l$) the convex relaxation will be exact with respect to PWL approximation. When the relaxation is locally tight, the controller has a meaningful and relatively accurate model of line losses, and hence of line temperature. This allows MPC to compute control actions that relieve line overloads.

Equations (24j) and (24k) denote nodal power balance constraints ($\forall i \in \mathcal{N}$) and DC power flows, respectively. Power balance is implied by Kirchhoff's law: power flowing into node i must equal the power flowing out plus/minus that injected/consumed. Note that the term $f_{ij,k}^{\text{loss,est}}$ in (24j) is a constant estimate of line losses at time-step k. It is shown in [30] that by decoupling this loss term from f_{ij}^{loss}, the PWL relaxation inherits crucial tightness properties. The "DC" power flow presented in (24k) couples lines flows to nodal phase angles.

Remark 3 (Fixing losses over the prediction horizon). Under the standard convex relaxation of a PWL approximation of line-losses [28], it is implicitly assumed, for tightness of the formulation, that nodal prices (i.e. LMPs) are non-negative. Negative nodal prices arise for nodes where increasing power consumption leads to decreased overall system costs. For example, if a line is congested or trips at time k and forces a generator at node i to decrease output (i.e. $f_{\text{G},i}[k] - f_{\text{G},i}[k-1] < 0$), then it can be shown that the nodal price at that node at time k will become negative. This breaks the assumption of non-negative nodal prices and prevents a tight formulation of losses. Fictitious losses can then "consume" power via the power balance equation (for nodes with negative LMPs) and reduce the overall objective function value. Similar but more thorough conclusions have been reached by authors in [29, 33] as it relates to convex relaxations in power systems.

To overcome the challenge of negative LMPs in this work, losses are fixed in (24j) to a value $f_{ij,k}^{\text{loss,est}}$ obtained from the most recent measurement of the AC system. The proof in [30] does not, therefore, require consideration of nodal prices. Furthermore, by fixing losses in the power balance equation, the network structure does not affect the convex relaxation. The astute reader will note that with losses fixed in (24j), the computed control actions will be slightly inconsistent with the actual AC system. However, this loss approximation typically constitutes less than 0.1% of total load, begets normalized line loss prediction errors of less than 5%, and is corrected by feedback in the MPC formulation.

Algebraic equations (24l), (24m), (24n) establish the relationship between

31

control inputs, namely demand response, storage injection/consumption, and wind curtailment, and the power balance of (24j).

The sets defined in (24o) and (24p) are convex polytopes. In particular, $\mathcal{X}$ is closed and $\mathcal{U}$ is compact:

$$\mathcal{X} = \left\{ x \big| E[l] \in [0, \overline{E}]; f_G[l] \in [\underline{f_G}, \overline{f_G}]; \Delta\hat{T}[l] \geqslant 0 \right\} \tag{26}$$

$$\mathcal{Z} = \Big\{ z \big| \theta_{ij}[l] \in [-\theta_{\max}, \theta_{\max}] \subset (-\pi/2, \pi/2); $$
$$\theta_{ij}^+[l], \theta_{ij}^-[l] \geqslant 0; \ \theta_{ij}^{\mathrm{PW}}(s)[l] \in [0, \Delta\theta] \Big\} \tag{27}$$

$$\mathcal{U} = \Big\{ u \big| f_{Dn}^{\mathrm{red}}[l] \in [0, \alpha_n^{\mathrm{red}}]; f_{G_Wn}^{\mathrm{spill}}[l] \in [0, \alpha_n^{\mathrm{spill}}]; $$
$$\Delta f_{Gn}[l] \in [-T_s R_n^{\mathrm{down}}, T_s R_n^{\mathrm{up}}]; $$
$$f_{Qc,n}[l] \in [0, \overline{f}_{Qc,n}]; f_{Qd,n}[l] \in [0, \overline{f}_{Qd,n}] \Big\} \tag{28}$$

with bounds defined by appropriate parameters. The sets contain the Level 1 reference trajectories $x^{\mathrm{sp}} \in \mathcal{X}, u^{\mathrm{sp}} \in \mathcal{U}$. Finally, the set $\mathcal{T}_x$ represents the convex polytopic terminal constraint set and is defined by:

$$\mathcal{T}_x = \left\{ x \big| \Delta\hat{T}[M] = 0 \wedge x[M] \in \mathcal{X} \right\} \subset \mathcal{X}. \tag{29}$$

Note that terminal constraints such as (29) may impact the feasibility of the QP problem if the chosen prediction horizon M is too short. In this work, M is appropriately chosen to ameliorate concerns of feasibility.

7.1.3. Enabling MPC to alleviate temperature overloads

To alleviate conductor temperature overloads, the convex relaxation of line losses must be tight whenever a line temperature rises above its limit (i.e. $\Delta T_{ij} > 0$). This condition is guaranteed by the theorem proven in [30], which also provides the full proof. To sketch the proof, let $\{\Delta T_{ij}[l]\}_{l=1}^M$ be an optimal MPC temperature trajectory for line (i, j) and assume $\exists\, l \in \mathcal{M}$ such that $\Delta T_{ij}[l+1] > 0$ but the solution is **not** tight for some $\kappa \leqslant l$. That is, losses are overestimated via the convex relaxation as shown in Fig. 7. Then a feasible solution can be derived which is identical to the optimal solution except that it enforces a tight formulation at time κ and reduces line losses accordingly, say from $f_{ij,\mathrm{relax}}^{\mathrm{loss}}[\kappa] > f_{ij,\mathrm{tight}}^{\mathrm{loss}}[\kappa]$. According to (24b), decreased losses at time κ result in lower temperature at later times, which implies that

the temperature overload at time $l + 1$ must be less under the tight feasible solution. Since the objective function penalizes $\Delta \hat{T}_{ij}[\kappa]$ and losses are fixed in power balance equation, the feasible tight trajectory provides a lower cost solution than the relaxed optimal trajectory. This is a contradiction. Thus, if (i, j) has a temperature overload at time $l + 1$, the formulation is locally tight $\forall \, \kappa \leqslant l$, which provides MPC with an accurate model of line losses and enables MPC to alleviate temperature overloads.

7.1.4. Mitigating simultaneous charging and discharging

This section compares the simple linear "simul-charge" energy storage model used in the receding-horizon MPC to the more accurate but (non-convex) complimentarity-based model. First, define the models' respective actions by the superscripts $(.)^S$ and $(.)^C$. Then, for a given optimal storage device action, f_Q^*, the following holds:

$$f_{Qc}^C[l] - f_{Qd}^C[l] =: f_Q^* := f_{Qc}^S[l] - f_{Qd}^S[l]. \tag{30}$$

Note that there exists only one unique complementarity-based control action (due to the condition $f_{Qc}^C[l] f_{Qd}^C[l] \equiv 0$). However, without complementarity (i.e. under the simultaneous charge/discharge formulation), multiple solutions may exist. One side-effect of allowing simultaneous charge/discharge events is identified by the following:

Theorem 4. *For a given optimal storage flow $f_Q^*[l]$, the simultaneous charge/discharge model (compared with the complementarity-based model) underestimates SOC (i.e. $\Delta E[l + 1] := E^C[l + 1] - E^S[l + 1]$) by*

$$\Delta E[l + 1] = T_s \frac{1 - \eta_c \eta_d}{\eta_d} \sum_{m=0}^{l} \min \left\{ f_{Qc}^S[m], f_{Qd}^S[m] \right\}. \tag{31}$$

Proof. The proof follows directly from considering the two cases: $f_{Qc}^C \equiv 0$ and $f_{Qd}^C \equiv 0$. $\qquad \square$

From the theorem, it is straightforward to see that the simultaneous charge/discharge model exactly matches the complementarity-based model when one of the following holds:

- $\eta_c = \eta_d = 1$ (perfect efficiency)

- $\min\{f_{Qc}^S[l], f_{Qd}^S[l]\} = 0$ (complementarity is satisfied)

- $f_Q^*[l] = \overline{f_Q}$

where $\overline{f_Q} \equiv \overline{f_{Qc}} = \overline{f_{Qd}}$ has been assumed for presentation clarity. (Generalization to $\overline{f_{Qc}} \neq \overline{f_{Qd}}$ is straightforward.) The last condition stems from

$$\min\{f_{Qc}^S[l], f_{Qd}^S[l]\} \in \left[0, \overline{f_Q} - f_Q^*[l]\right]. \tag{32}$$

This means that the controller can (erroneously) employ simultaneous charge/discharge to achieve a lower-than-actual SOC, which could be advantageous to reduce the cost of SOC deviations from the Level 1 reference. Furthermore, the controller can utilize simultaneous charge/discharge to reduce line overloads by fictitiously "burning" excess power through energy storage inefficiencies ($\eta_c, \eta_d < 1$).

To reduce the effect and occurrence of simultaneous charge/discharge events, two steps have been implemented. Firstly, to reduce the worst-case behavior of the simultaneous charge/discharge formulation, the following constraint is utilized:

$$\frac{f_{Qc,n}[l]}{\overline{f_{Qc,n}}} + \frac{f_{Qd,n}[l]}{\overline{f_{Qd,n}}} \leqslant 1 \qquad \forall l, n, \tag{33}$$

where $\overline{f_{Qc,n}}$, $\overline{f_{Qd,n}}$ are the rate limits on charging and discharging, respectively.

Secondly, most devices at most time-steps will satisfy $f_{Qn}[l|k] \neq 0$. This knowledge can be used to enforce complementarity-like constraints, and limit occurrences of simultaneous charge/discharge events. When MPC first runs, the charge/discharge status of storage devices over the prediction horizon is most likely unknown. In order to initialize the status, simultaneous charging/discharging is permitted for that first prediction trajectory. When MPC next runs, at time k, the charge/discharge status of each storage device over the prediction horizon is determined from its status at the corresponding time-step in the previous prediction trajectory (i.e. $k - 1$). It should be noted that the prediction horizon at time-step $k - 1$ only extends to $f_{Qn}[M - 1|k - 1]$, so no prior value is available for initializing the status of $f_{Qc,n}[M - 1|k]$ and $f_{Qd,n}[M - 1|k]$. Therefore, the Level 1 status at the corresponding time can be used to establish the charging state for all devices at this terminal time-step. Fig. 9 outlines the algorithm employed in MPC.

Remark 5. This algorithm introduces a delay of one time-step in the transition of storage devices from charging to discharging, or vice-versa. To

1: *Initialize:* set $\alpha_{tol} \geqslant 0$
2: **if** $k = 0$ **then**   ▷ MPC first run: allow simulcharge
3:     **for** $l = 0, 1, \ldots, M - 1$ **do**
4:         $f_{Qc,n}[l|k], f_{Qd,n}[l|k]$ satisfy (33)
5:     **end for**
6: **else**
7:     **for** $l = 0, 1, \ldots, M - 2$ **do**
8:         **if** $f_{Qn}[l + 1|k - 1] > \alpha_{tol}$ **then**
9:             $f_{Qd,n}[l|k] = 0, f_{Qc,n}[l|k] \in [0, \overline{f_{Qc,n}}]$
10:         **else if** $f_{Qn}[l + 1|k - 1] < -\alpha_{tol}$ **then**
11:             $f_{Qc,n}[l|k] = 0, f_{Qd,n}[l|k] \in [0, \overline{f_{Qd,n}}]$
12:         **else**   ▷ Possible transition: allow simulcharge
13:             $f_{Qc,n}[l|k], f_{Qd,n}[l|k]$ satisfy (33)
14:         **end if**
15:     **end for**   ▷ Terminal control
16:     set $f_{Qc,n}[M - 1|k] = 0, f_{Qd,n}[M - 1|k] = 0$ according to Level 1
17: **end if**

Figure 9: Reducing the effect of simultaneous charge/discharge for Level 2 MPC at time-step k.

address this issue, computation of the MPC trajectory for time k can be repeated using the latest status information. At this re-run, storage devices with $f_{Qn}[l|k] \in [-\alpha_{tol}, \alpha_{tol}]$ are handled in accordance with line 13 in Fig. 9.

To summarize, constraint (33) limits the worst-case behavior of simultaneous charge/discharge, and the algorithm in Fig. 9 reduces the frequency of simultaneous charge/discharge events. The methodology of the proposed simul-charge algorithm is illustrated in Fig. 10. The red arrows represent the original complementarity-based (non-convex) model, while the green region represents effect of constraint (33). The total impact of the heuristic is given by union of red arrows and dashed red line, which represents the admissible set of storage behaviors. Thus, by shrinking the simul-charge area from the green-blue rectangle to just the red dashed line, the heuristic makes the storage model more representative of reality, but at a slightly increased computational cost.
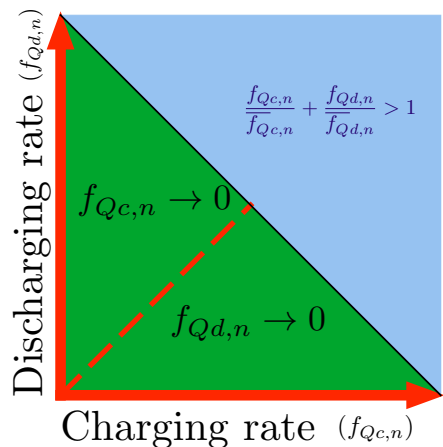
Figure 10: Visualizing the effects of the heuristic proposed in Fig. 9 to reduce severity of simultaneous charging and discharging in MPC scheme.

7.2. Base-case Controller

To benchmark the performance of the proposed MPC scheme, a base-case controller was developed. This base-case was meant to provide an indication of human operator behavior during a system emergency (disturbance). Clearly, modeling a human operator is non-trivial as standard emergency procedures vary broadly across utilities. Furthermore, the experience of a human operator is not amenable to an implementable (and repeatable) algorithmic framework and, as far as the authors are aware, no data-sets exist which captures operator behavior during (simulated) contingencies. However, the formulation presented here captures the underlying goals of the operator:

1. alleviate thermal overloads by rescheduling or curtailing generation, while considering ramp-rate limits and incremental generator cost curves,
2. employ sensitivity-based methods, such as power transmission distribution factors (PTDFs), generation shift factors (GSFs), and transmission loading relief (TLR) procedures to make quick control decisions to relieve thermal overloads [34],
3. shed load as an absolute last resort, and
4. ignore energy storage.

Thus, mapping the above operator traits into an MPC-based framework serves as the base-case:

- **Base-case implementation**

  - Replace $\Delta \hat{T}_{ij}[l]$ with a relative overload metric:

  $$\hat{o}_{ij}[l] = 10 \max\{0, (|f_{ij}[l]| + 0.5 f_{ij}^{loss}[l])/f_{ij}^{\lim} - 1\} \qquad (34)$$

  That is, if a line is 25% overloaded, $\hat{o}_{ij} = 2.5$.

  - Consider PTDF, GSF, and TLR implicitly as a 1-step linear MPC process akin to Level 2 (i.e. set $M = 1$) and include overloads $\hat{o}_{ij}[0|k]$, $\hat{o}_{ij}[1|k]$ in the objective and terminal costs.
  - Heavily penalize load control and adjustment of SOC.
  - Remove terminal constraints on overloads, $\mathcal{T}_x$.
  - Set weighting matrices $R_{\text{base}} = R$, $Q_{\text{base}} = S_M$, $S_{M,\text{base}} = S_M$.

7.3. Actual system model (plant)

The AC power flow is generally accepted as a valid representation of the actual physical power system (i.e. the plant). Therefore, the control actions recommended by the MPC, which utilizes the strictly linear model described in Section 7.1.2, is applied to an AC model of the system at each time-step. This interaction between predictive DC controller and actual AC plant is illustrated in Fig. 11. Furthermore, the resulting losses from the AC power flow are utilized in the nonlinear IEEE Standard 738 conductor temperature model to better capture the effects of MPC recommendations on the actual system. Finally, the actual energy storage model does not allow for simultaneous charging and discharging in the same time-step and instead employs the projected control action $f_{Qn}[k]$ such that $f_{Qc,n}[k]f_{Qd,n}[k] \equiv 0$.

The higher the temperature, the more likely line tripping becomes. To capture the inverse relationship between temperature and expected time to trip in the actual system, the probabilistic thermal line outage model from Section 4.1.1 is employed.

7.4. Case Study: IEEE RTS-96

The bilevel control scheme is applied to an augmented version of the IEEE RTS-96 power system test-case, which is described in full details in [35]. A brief overview of this test-case is included here.
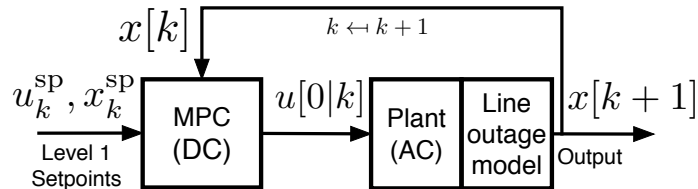
Figure 11: Interaction of Level 2 MPC with the grid.

7.4.1. Overview

The IEEE RTS-96 system consists of 138 kV and 230 kV subsystems. The network is organized into three interconnected physical regions, as illustrated in Fig. 12. It consists of 73 nodes and 120 branches, of which 15 branches are tap-changing transformers, one is a phase-shifting transformer[7], and the remainder are overhead transmission lines (138 and 230 kV). Buses are denoted with three digits: the first digit indicates the area while the latter two are intra-area designators. Bus types are indicated by color: generator (blue), load (yellow), and zero-injection (white). Edges represent transmission lines (black) and transformers (aqua/gray). The disturbance is displayed with stars: lines 113-215 and 123-217 were tripped. Note that the three underground cables in the original RTS-96 system have been replaced by equivalent overhead lines to enable application of a single thermodynamic model. Transformer temperature overloading is not considered in this case study, as their thermodynamic models differ from those of overhead transmission lines.

The aim of this case study is to explore the contingency management achievable with the proposed hierarchical control scheme. Unfortunately, the RTS-96 system is designed as a highly reliable system, with unusually high thermal ratings for lines. To bring the system closer to its limits and engender worthwhile scenarios, thermal ratings $f_{ij}^{\lim}$ were reduced by 40%, yielding line temperature limits in the range of 60-70°C. Furthermore, ramp-rates have been reduced by 82.5% to highlight Level 2 performance and enhance the role of storage in congestion management. For the temperature dynamics, the RTS-96 system data only specifies per-unit resistance, reactance and line length, but not the conductor types (i.e. diameter, heat capacity). Therefore, this case-study employed ACSR conductors, 18/1 Waxwing (138 kV) and

---

[7]Transformers modify power flows but can be accounted for within a unified power flow framework as was done in [30].
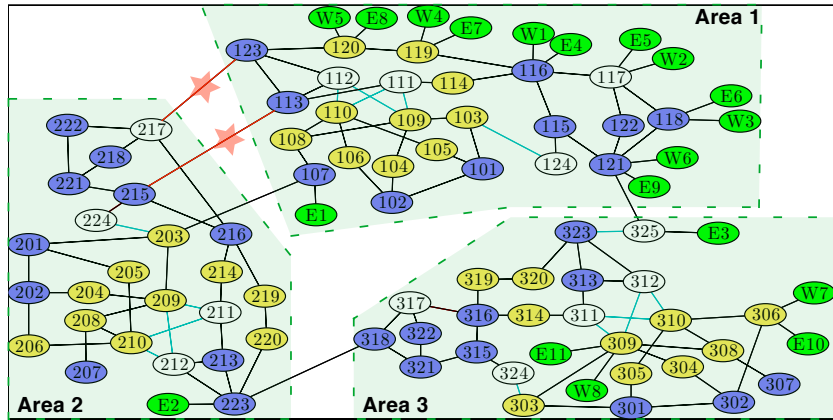
Figure 12: Modified IEEE RTS-96 network with storage (E) and wind (W) included. Note that storage and wind resources are associated with buses, as indicated in the figure, but the respective edges do not represent transmission lines.
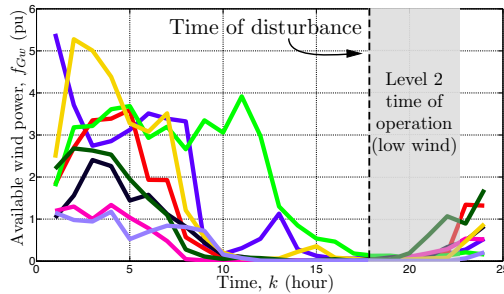

Figure 13: Hourly wind power profiles for 8 wind turbines in the RTS-96 network over a 24-hour horizon.

26/7 Dove (230 kV), which represent reasonable choices given the reduced line ratings. The parameter values for Dove and Waxwing conductors, along with other system parameters, are provided in Table 1. Values in brackets represent ranges.

7.4.2. Optimization implementation

The objective function weighting factors utilized in MPC Level 2 and the base-case are presented in Table 2. Note that for the base-case, the overload coefficient p_o weights the thermal power overload, $\hat{o}_{ij}$, and not temperature. Also, the storage control coefficient for the base-case, $p_q = 1000$, reflects the fact that this resource is not available for decision-making. Generator

Table 1: Network model parameters used in case-study.

Model Parameter	Value		Units
Sampling Time, T_s	60		s
3-phase power base, S_b	100		MVA
Energy storage base, E_b	100		MWh
Monetary unit base, M_b	10,000		$
Storage SOC limits, $\overline{E}_i$	2		pu
Storage power limits, $\overline{f}_{Qc}, \overline{f}_{Qd}$	0.25		pu
Nominal wind power, f_{GW}^{nom}	Fig. 13		pu
Nominal loads, $f_{\mathrm{D}}^{\mathrm{nom}}$	Week 1, day 1 in [35]		pu
Overcurrent protection limit, $\overline{\Omega}$	3		-
Ambient Temperature, T_{amb}	35		$^\circ$C
Wind speed, angle, $v_w \angle \theta_w$	$0.61, \pi/2$		m/s, rads
Line-to-line base voltage, V_b	138	230	kV
Thermal rating, f_{ij}^{lim}	1.05	3.00	pu
Conductor diameter, D_{ij}	15.5	23.5	mm
Heat capacity, $mC_{p,ij}$	383	916	J/m-$^\circ$C
Ampacity, I_{ij}^{lim}	439	753	A
Resistance per unit length, R_{ij}	[103,118]	[55,66]	$\mu\Omega$/m
Temperature limit, T_{ij}^{lim}	[62,64]	[67,71]	$^\circ$C
Temperature coefficient, τ_{ij}	0.796	0.888	-
Loss coefficient, ρ_{ij}	0.157	0.066	$^\circ$C-m/W
Ambient coefficient, γ_{ij}	0.193	0.104	-
Solar heat gain rate, $q_{s,ij}$	14.4	21.9	W/m

Table 2: Objective function coefficients for Q, R, S_M matrices for MPC and base-case systems.

Model	p_o	p_e	p_g	p_r	p_w	p_s	p_q	p_p
Level 2 MPC	1	200	200	[0.05,1]	0.15	250	0.2	0.01
Base Case	1	0.01	0.01	[0.01,0.1]	0.5	500	1000	0.1

control actions, Δf_G, are weighted using cost curve parameters[8], with $p_r = \max\{0.05, a_n/\max_n\{a_n\}\}$ for Level 2, and $p_r = 0.1\max\{0.1, a_n/\max_n\{a_n\}\}$ for the base-case. The cost-curve parameters (a_n, b_n) utilized in this case-study are from [36, Table 1].

Recall, that the early stages of a cascade evolve relatively slowly, which allows for significant computation to be performed during that period. Therefore, immediately following a disturbance, Level 1 computes new optimal set-points and passes that updated information to Level 2. An overview of Level 2 operation is displayed in Fig. 11.

7.4.3. Simulation Results

The case-study described in Section 7.4.1 is simulated in Matlab according to Level 1, Level 2, and base-case implementations. Initially, the system is operated economically according to Level 1. However, at hour 18 (low wind, high demand), a two-line outage (i.e. the disturbance) trips lines 113-215 and 123-217. Transient (short-term) stability was assumed. Performance and behavior of the Level 2 MPC (with horizon lengths of $M = 5, 10, 20, 30,$ and 45) and the base-case are discussed below.

The double-line outage caused the remaining inter-area transmission line 107-203 to become severely overloaded (greater than $1.25 f_{ij}^{\mathrm{lim}}$). The Level 2 MPC scheme alleviated the temperature overloads and brought the system safely to the updated economic set-points provided by Level 1. In contrast, the base-case underwent a cascading failure, with line tripping bringing the system to a voltage collapse after 29 minutes, as exemplified by non-convergence of the AC power flow. The base-case cascading failure evolved as follows:

- $k = 3$: line 107-203 tripped at $\Delta T_{ij}[3] = 13.5\,°\mathrm{C}$.

- $k = 16$: line 114-116 tripped at $8.14\,°\mathrm{C}$.

- $k = 26$: line 113-123 tripped at $11.4\,°\mathrm{C}$.

- $k = 28$: lines 103-109 and 112-123 tripped at $16.8\,°\mathrm{C}$ and $20.7\,°\mathrm{C}$.

- $k = 29$: voltage collapse "Blackout".

---

[8]Recall that the generator cost curves used in Level 1 are of the form: $\mathrm{Cost}(f_{Gn}[k]) = a_n(f_{Gn}[k])^2 + b_n f_{Gn}[k]$.
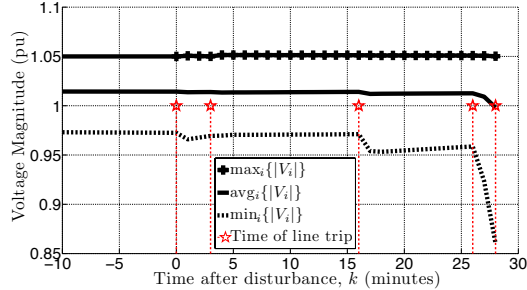
Figure 14: Base-case operation: voltages undergo cascading failure, resulting in voltage collapse.

This process is illustrated in Fig. 14, where it can be seen that the minimum voltage magnitude fell below 0.87 pu.

Fig. 15a illustrates that the objective function cost (18a), calculated for each MPC run, decreased monotonically over time. This does not prove stability, but highlights the Lyapunov-like properties of the objective function [7] as MPC drives the system back to the Level 1 (economically optimal) equilibrium point.

The maximum line temperatures for the base-case and MPC are illustrated in Fig. 15b. Note that MPC is able to avoid excessively high temperatures, and in fact drives all line temperatures below their respective limits by around minute $k \approx 75$. Later, a few lines hover slightly above their temperature limits. However, this is due to model inaccuracy arising from MPC's use of an approximate linear temperature model and the DC power flow. In particular, over that latter phase, the largest temperature deviations above limits are associated with 138 kV lines that exhibit $X/R = 3.83 < 4$. This relatively low X/R ratio engenders errors in the DC approximation of the nonlinear AC network equations. The DC model incorrectly informs the controller that losses are sufficiently low, implying that negligible control action is required for the temperature to drop below its limit in the next time-step. But the actual power system, described by the AC power flow, has higher than predicted losses, and the temperature stays slightly above the limit. The controller repeats these incorrect estimates of losses until control action is required for other reasons, or load patterns autonomously reduce line loadings below limits. For $k > 50$, all line loadings are less than 5% above their thermal ratings, which is within expected error levels [37, 38]. These results suggest that despite the presence of approximate models, the MPC

42

scheme is able to reject the disturbance through feedback and return the system to an acceptable state. A thorough discussion of the impact of model approximations is provided in [39].

Level 2 MPC performs a balancing act between ensuring safety criteria and restoring economically optimal set-points. This balance is highlighted in Fig. 15c, where the cost of conventional generation is shown for both MPC and the base-case. To ensure acceptable line temperatures, MPC initially sacrifices economic optimality by deviating from the Level 1 set-points. For $k > 120$, the system returns to economically optimal levels, with inaccuracy in the MPC model causing some minor discrepancies. Interestingly, over the first 15 minutes or so, the generation cost achieved by MPC is actually less than the optimal cost given by Level 1. Two factors contribute to this apparent anomaly. Firstly, Fig. 15c shows the post-disturbance Level 1 schedule, whereas the generators were initially operating according to less-costly pre-disturbance set-points. Secondly, the updated Level 1 reference schedule enforces hard line-flow constraints, while MPC allows line flows to temporarily exceed limits.

As discussed in Section 7.1, the control actions available to Level 2 MPC for reducing line temperatures include: load reduction, wind curtailment, and energy storage injections. Figs. 15d and 15e illustrate the main controls employed to alleviate excessive temperatures for this case-study. Contrasting MPC response with the base-case, it is clear that load and energy storage controls were crucial immediately following the disturbance. By initially curtailing energy storage discharge (Fig. 15d) and reducing the aggregate load by less than 5% (Fig. 15e), line temperatures were brought to within their limits. For $k \in [75, 240]$, storage discharge exceeded reference levels in order to bring SOC back to economical reference levels as displayed in Fig. 15f. Wind curtailment was employed as cheap control over the longer term to bring and keep line temperatures below their limits.

Finally, with a shorter horizon M and the terminal constraint requiring greater use of expensive load and storage control, the MPC enjoys smaller departures in generation from the Level 1 economic reference. Such an outcome is displayed in the generation costs of Fig. 15c. However, with a short horizon (e.g. $M = 5$), the controller is unable to predict the line overloads far enough in advance, which causes inferior management of energy storage and load. For example, notice in Fig. 15f how much further away from the Level 1 reference the MPC with horizon $M = 5$ is compared with $M \geqslant 10$. Considering the degree of load and storage control and line temperature pro-
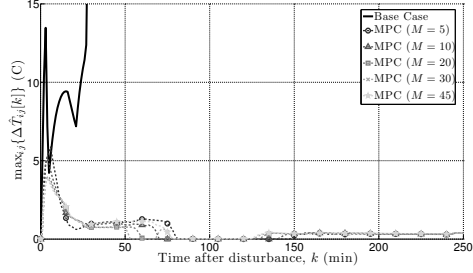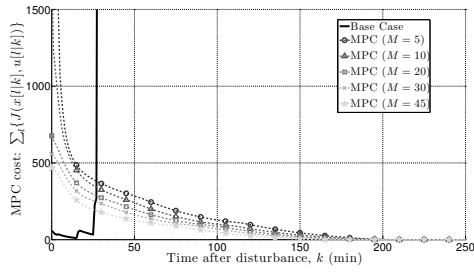
(a) Total MPC objective function value. (b) Maximum line temperature responses.
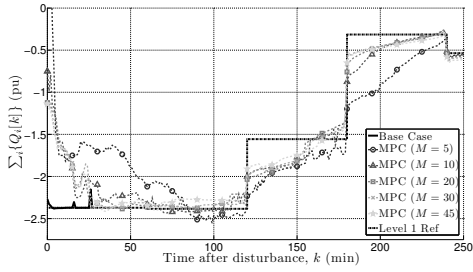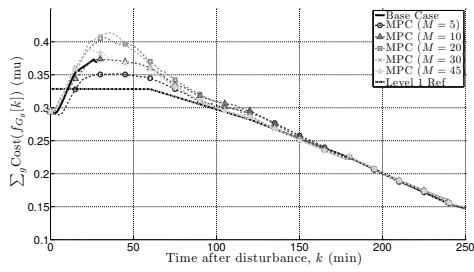
(c) Total cost of generation with reference (d) Aggregate charging and discharging.
from Level 1.
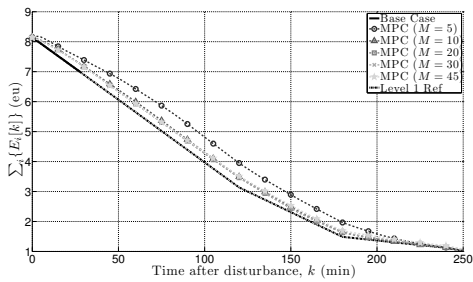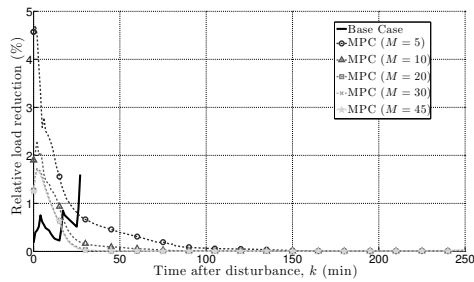
(e) Aggregate load control. (f) Aggregate storage SOC.

Figure 15: Case-study simulation results for MPC and the base-case.

44

files, a prediction horizon of $M = 20$ provides the best sacrifice between computational complexity and controller performance.

7.5. Data management and communication

The MPC control scheme requires a model of the network, together with measurements of the conductor temperature of (potentially) overloaded lines, SOC of energy storage devices, output power from both conventional and renewable generation, power demand, and the operating points of all FACTS devices would be required. These data establish the initial point for the MPC prediction trajectory, and therefore must be updated every time MPC reinitializes, at the time-step T_s. These measurement requirements are consistent with existing energy management system (EMS) capabilities, with topology processing establishing the network model, and state-estimation providing generation and load information. Technology for measuring conductor temperature is available, though telemetry of such measurements is not currently common. It is argued in [14] and references therein, in the context of dynamic line rating, that gathering line temperatures is quite feasible. Also, a trivial modification to the MPC formulation would allow some lines to be subject to standard (hard) power flow limits, while modeling temperature dynamics for lines that were outfitted with temperature sensors. Participation of energy storage devices in electricity markets will likely require telemetry of their SOC. This is already the case in NYISO [40] and PJM [41].

In addition to well defined initial conditions, MPC prediction also requires forecasts of demand, the power available from renewable generation sources, and the ambient weather conditions governing line temperatures. Generation and load forecasts are already available and used in EMS contingency analysis. Short-term weather forecasts are also typically available. Given that the MPC prediction horizon will generally be on the order of 15-30 minutes, a persistence forecast (which assumes those external influences remain unchanged) will often be adequate but more advanced very-short-term load forecasting techniques can be applied if necessary [42].

MPC broadcasts control signals at an interval of $T_s \approx 1$ minute, which is much slower than other controls, such as AGC [43]. Thus the input/output communications and data management requirements of the MPC scheme are consistent with the capabilities of existing EMS installations.

8. Summary

This chapter describes the active role of energy storage in a cascade mitigation scheme, which leverages the benefits of model-predictive control (MPC) while simple linear models greatly reduce MPC's computational requirements. The MPC scheme balances economic and security objectives through the use of a higher-level optimal economical scheduling process and a lower-level MPC corrective strategy.

The notion of cascade mitigation is advanced by the development of a receding horizon MPC cascade mitigation scheme applied to electric transmission systems with energy storage. The MPC design rejects disturbances (contingencies) while tracking the optimal set-points established by the higher economical level. The controller exploits the thermal overload capability of transmission lines. This allows time for adjustments to be made to controllable resources that include generation levels, energy storage and demand response. A convex relaxation is applied to the AC power flow to develop a linear approximation for line losses. This formulation is proven to be sufficient to enable MPC to drive line temperatures below limits. As supported by an augmented IEEE RTS-96 case study, the MPC scheme can significantly improve system reliability and economic performance by leveraging the temporal nature of energy storage and conductor temperatures.

9. References

[1] W. A. Wulf, "Great achievements and grand challenges," *National Academy of Engineering - The Bridge*, vol. 30, pp. 5–10, Oct 2000.

[2] "Grid 2030 - a national vision for electricity's second 100 years," tech. rep., Federal Energy Regulatory Commission, July 2003.

[3] M. Geidl, G. Koeppel, P. Favre-Perrod, B. Klockl, G. Andersson, and K. Fröhlich, "Energy hubs for the future," *IEEE Power & Energy Magazine*, vol. 5, no. 1, pp. 24 – 30, 2007.

[4] M. Geidl and G. Andersson, "Operational and topological optimization of multi-carrier energy systems," *International Conference on Future Power Systems*, pp. 6 pp. – 6, 2005.

[5] A. del Real, M. D. Galus, C. Bordons, and G. Andersson, "Optimal power dispatch of energy networks including external power exchange," *IEEE Euro-*

pean Control Conference, vol. 9, 2009. energy hubs, optimal dispatch, power flow.

[6] "Final report on the August 14, 2003 blackout in the United States and Canada: Causes and recommendations," tech. rep., US-Canada Power System Outage Task Force, Apr 2004.

[7] D. Mayne, J. Rawlings, C. V. Rao, and P. O. M. Scokaert, "Constrained model predictive control: Stability and optimality," *Automatica*, vol. 36, no. 6, pp. 789–814, 2000.

[8] F. Borrelli, A. Bemporad, and M. Morari, *Predictive Control for Linear and Hybrid Systems*. Cambridge, U.K.: Cambridge Univ. Press, 2011. version update: Apr. 22, 2014.

[9] G. Goodwin, M. Seron, and J. De Doná, *Constrained Control and Estimation: An Optimisation Approach*. Communications and control engineering series, Springer Science & Business Media, 2005.

[10] M. Larsson, D. J. Hill, and G. Olsson, "Emergency voltage control using search and predictive control," *Electrical Power and Energy Systems*, vol. 24, pp. 121–130, Feb 2002.

[11] M. Zima, P. Korba, and G. Andersson, "Power systems voltage emergency control approach using trajectory sensitivities," *IEEE Conference on Control Applications*, pp. 189 – 194, 2003.

[12] I. A. Hiskens and B. Gong, "MPC-based load shedding for voltage stability enhancement," *IEEE Conference on Decision and Control*, Dec 2005.

[13] P. Hines and S. Talukdar, "Controlling cascading failures with cooperative autonomous agents," *International journal of critical infrastructures*, vol. 3, no. 1, pp. 192–220, 2007.

[14] H. Banakar, N. Alguacil, and F. D. Galiana, "Electrothermal coordination part I: Theory and implementation schemes," *IEEE Transactions on Power Systems*, vol. 20, pp. 798–805, May 2005.

[15] N. Alguacil, H. Banakar, and F. D. Galiana, "Electrothermal coordination part II: Case studies," *IEEE Transactions on Power Systems*, vol. 20, pp. 1738–1745, Nov 2005.

[16] B. Otomega, A. Marinakis, M. Glavic, and T. Van Cutsem, "Emergency alleviation of thermal overloads using model predictive control," *PowerTech*, pp. 201–206, Jun 2007.

[17] J. Carneiro and L. Ferrarini, "Preventing thermal overloads in transmission circuits via model predictive control," *IEEE Transactions on Control Systems Technology*, vol. 18, no. 6, pp. 1406 – 1412, 2010.

[18] M. Almassalkhi and I. A. Hiskens, "Cascade mitigation in energy hub networks," *IEEE Conference on Decision and Control*, Dec 2011.

[19] D. Bienstock and S. Mattia, "Using mixed-integer programming to solve power grid blackout problems," *Discrete Optimization*, vol. 4, pp. 115–141, Mar 2007.

[20] B. Carreras, V. Lynch, M. Sachtjen, and I. Dobson, "Modeling blackout dynamics in power transmission networks with simple structure," *IC SS*, Jan 2001.

[21] IEEE Standard 738, *IEEE Standard for Calculating the Current-Temperature of Bare Overhead Conductors*, 2007.

[22] D. Mohanty, "Jumbo deaths: It is time to act." *The Indian Express*, Available: http://www.indianexpress.com/news/jumbo-deaths-it-is-time-to-act/1053724/ [Last accessed: 1 June 2014].

[23] L. Bahiense, C. Oliveira, M. Pereira, and S. Granville, "A mixed integer disjunctive model for transmission network expansion," *IEEE Transactions on Power Systems*, vol. 16, no. 3, pp. 560–565, 2001.

[24] D. Braess, "Über ein paradoxon aus der verkehrsplanung," *Unternehmensforschung*, no. 12, pp. 258–268, 1968.

[25] M. Geidl and G. Andersson, "Optimal power flow of multiple energy carriers," *IEEE Transactions on Power Systems*, vol. 22, no. 1, pp. 145 – 155, 2007.

[26] M. Almassalkhi and I. A. Hiskens, "Optimization framework for the analysis of large-scale networks of energy hubs," *Power Systems Computation Conference*, Aug 2011.

[27] M. Almassalkhi and I. A. Hiskens, "Impact of energy storage on cascade mitigation in multi-energy systems," *IEEE PES General Meeting*, Jul 2012.

[28] A. L. Motto, F. D. Galiana, A. J. Conejo, and J. M. Arroyo, "Network-constrained multiperiod auction for a pool-based electricity market," *IEEE Transactions on Power Systems*, vol. 17, pp. 646–653, Aug 2002.

[29] R. Palma-Benhke, A. Philpott, A. Jofré, and M. Cortés-Carmona, "Modelling network constrained economic dispatch problems," *Optimization and Engineering*, pp. 1–14, Oct 2012.

[30] M. Almassalkhi and I. Hiskens, "Model-predictive cascade mitigation in electric power systems with storage and renewables part I: Theory and implementation scheme," *IEEE Transactions on Power Systems*, to appear, 2014.

[31] D. Bienstock and A. Verma, "The n-k problem in power grids: New models, formulations, and numerical experiments," *SIAM Journal on Optimization*, vol. 20, p. 2352, 2010.

[32] A. Wood and B. Wollenberg, *Power Generation, Operation, and Control*. Wiley-Interscience, second ed., 1996.

[33] B. Lesieutre, D. Molzahn, A. Borden, and C. L. Demarco, "Examining the limits of the application of semidefinite programming to power flow problems," *Allerton Conference*, pp. 1492–1499, Oct 2011.

[34] Operations Support Division, "Manual on transmission operations," tech. rep., PJM, Dec 2012.

[35] C. Grigg, P. Wong, P. Albrecht, R. Allan, M. Bhavaraju, R. Billinton, Q. Chen, C. Fong, S. Haddad, S. Kuruganty, W. Li, R. Mukerji, D. Patton, N. Rau, D. Reppen, A. Schneider, M. Shahidehpour, and C. Singh, "The IEEE reliability test system," *IEEE Transactions on Power Systems*, vol. 14, no. 3, pp. 1010 – 1020, 1999.

[36] H. Chavez and R. Baldick, "Inertia and governor ramp rate constrained economic dispatch to assess primary frequency response adequacy," *International Conference on Renewable Energies and Power Quality*, Mar 2012.

[37] T. J. Overbye, X. Cheng, and Y. Sun, "A comparison of the AC and DC power flow models for LMP calculations," *IEEE Hawaii International Conference on System Sciences*, Jan 2004.

[38] B. Stott, J. Jardim, and O. Alsaç, "DC Power Flow Revisited," *IEEE Transactions on Power Systems*, vol. 24, no. 3, pp. 1290–1300, 2009.

[39] M. Almassalkhi and I. Hiskens, "Model-predictive cascade mitigation in electric power systems with storage and renewables part II: Case-study," *IEEE Transactions on Power Systems*, to appear, 2014.

[40] D. Allen, C. Brown, J. Hickey, V. Le, and R. Safuto, "Energy storage in the New York electricity market," tech. rep., NYISO, Dec 2009.

[41] PJM Interconnection Planning Committee, "Energy Storage: Technologies Ready for the Market," Presented at the Electricity Storage Association, Oct 2013.

[42] C. Guan, P. B. Lu, L. D. Michel, Y. Wang, and P. B. Friedland, "Very short-term load forecasting: Wavelet neural networks with data pre-filtering," *IEEE Transactions on Power Systems*, vol. 28, pp. 30–41, May 2013.

[43] N. Jaleeli, L. VanSlyck, D. Ewart, L. Fink, and A. Hoffmann, "Understanding automatic generation control," *IEEE Transactions on Power Systems*, vol. 7, pp. 1106–1122, August 1992.